Environmental Science: Atmospheres

ROYAL SOCIETY OF CHEMISTRY

PAPER

View Article Online
View Journal

Cite this: DOI: 10.1039/d6ea00019c

Source apportionment and driving mechanisms of black carbon in a mountainous megacity: insights from urban–suburban observations in Chongqing, China

Yimei Wang,†[ab] Junjie Ding,†[abc] Jie Zhao,[ab] Peng Zhang,[ac] Jun Chen,[a] Wei Huang,[ac] Xin Zhang,[ab] Xi Pu,[ac] Mengyao Wang,[ac] Pengrui Fu[a] and Jiayan Yu *[abc]

Black carbon, a strongly light-absorbing aerosol from incomplete combustion, has raised global concern due to its substantial impacts on climate forcing, air quality degradation, and public health risks. This study investigates the distribution and sources of equivalent BC (eBC) across urban–suburban sites in Chongqing, a mountainous megacity in southwestern China, based on year-long multi-wavelength Aethalometer (AE33) observations. Four sites were deliberately selected to represent distinct source regimes—port, airport, rail freight, and dense urban traffic—in a spatial source separation design. Annual mean eBC concentrations ranged from 2.4 ± 1.3 μg m^{-3} at the urban site to 2.8 ± 1.9 μg m^{-3} in suburban areas. Using absorption Ångström exponent diagnostics, eBC was apportioned into traffic-related (eBC_{liquid}) and biomass/coal-burning (eBC_{solid}) components. Results showed distinct spatiotemporal patterns between the two components: eBC_{liquid} dominated urban area (up to 85%) and was significantly elevated during weekdays ($p < 0.0001$), while eBC_{solid} exhibited a pronounced wintertime enhancement in suburban areas, accounting for nearly 40% of total eBC, indicating the influence of seasonal solid fuel combustion. Seasonally resolved correlation analysis further revealed that source–tracer relationships, such as the eBC_{liquid}–AAE correlation at the port site, shifted markedly with season, capturing the transition from shipping-dominated emissions in summer to mixed solid fuel influences in winter. Notably, riverine freight activity during the flood season contributed to episodic increases in eBC_{liquid}. Local meteorological factors, especially wind and temperature, substantially modulated eBC accumulation and dispersion. Strong correlations with NO_x, SO_2, and NMHCs further improved the source attribution. These findings underscore the heterogeneous behaviors of eBC components under complex terrain–meteorology interactions and provide region-specific evidence for emission control. The results suggest that strengthening traffic management in urban cores and promoting clean energy substitution in suburban areas are essential to reduce BC pollution and improve air quality in mountainous megacities.

Received 3rd February 2026
Accepted 20th May 2026

DOI: 10.1039/d6ea00019c

rsc.li/esatmospheres

Environmental significance

Black carbon (BC) is a key short-lived climate pollutant and health-relevant aerosol that remains insufficiently characterized in rapidly urbanizing and topographically complex regions. This study provides process-level insights into BC source attribution and behavior across an urban–suburban gradient in Chongqing, a mountainous megacity in southwestern China. Our year-long, multi-site analysis reveals how traffic, biomass combustion, and riverine freight activities shape BC dynamics under seasonal meteorological modulation. These findings identify spatially and temporally specific intervention windows for pollution control, informing evidence-based strategies in terrain-influenced urban environments.

1 Introduction

Black carbon (BC), a strongly light-absorbing aerosol primarily emitted from incomplete combustion (*e.g.*, fossil fuels and biofuel), has attracted global attention due to its significant impacts on climate warming and public health deterioration.[1] As the second most potent climate forcer after CO_2, BC

[a]*Chongqing Ecological Environment Monitoring Center, Chongqing, 401147, China*
[b]*Key Laboratory of Atmospheric Pollution Causes, Prevention and Control in Complex Terrain of Chengdu-Chongqing Region, Ministry of Ecology and Environment, 401147, China. E-mail: yimeiwang@klapc.org.cn; j.j.ding@foxmail.com; jiayan.yu@klapc.org.cn*
[c]*Chongqing Ecological Environment Key Laboratory of Cause Analysis and Decision Support of Atmospheric Pollution, Chongqing, 401147, China*
† These authors contributed equally to this paper.

contributes substantially to atmospheric warming through direct radiative forcing and snow/ice albedo reduction.[2,3] It is also a key component of $PM_{2.5}$ and has been strongly associated with adverse health outcomes, including respiratory, cardiovascular, and neurological disorders.[4,5] BC also worsens haze by suppressing vertical pollutant dispersion.[6,7] Its morphology and surface area promote aerosol interactions and reactive chemistry.[8–10] Recognized as a short-lived climate pollutant (SLCP) by the World Health Organization[11] and the Climate and Clean Air Coalition,[12] BC is a critical target for mitigation efforts that deliver near-term co-benefits for both climate stabilization and air quality improvement. Comprehensive BC monitoring remains vital in densely populated regions with complex sources.

China, as one of the largest global BC emitters,[13,14] faces persistent challenges in balancing pollution control and economic growth. While national policies have led to notable reductions in $PM_{2.5}$ concentrations in recent years,[15,16] the carbonaceous fractions in $PM_{2.5}$ (BC, BrC, and OC) remain high in urban areas,[17,18] as water-soluble inorganic fractions decline.[19,20] These carbonaceous components originate from diverse sources including road traffic, riverine freight, residential combustion of coal and biomass, and secondary organic aerosol (SOA) formation from volatile organic compounds (VOCs).[21] In many cities, transportation accounts for over 70% of urban BC, underscoring liquid fossil fuel dominance in densely populated regions.[22–25] Chongqing, the largest city in western China, exemplifies these issues. Its high BC emissions are exacerbated by complex terrain, frequent stagnation, and meteorological inversions, leading to pollutant accumulation.[14,26–28] Dense transportation sources (*e.g.*, road-traffic, riverine freight traffic) and seasonal combustion (*e.g.*, biomass burning, meat curing) compound pollution.[29–31] Moreover, frequent stagnation enhances BC aging and absorption, complicating source attribution.[32,33]

Although BC has been widely studied in megacities,[34–39] multi-site observations remain scarce in topographically complex regions like southwestern China.[40] Mountain-basin meteorology limits atmospheric mixing, driving spatial heterogeneity in BC levels.[41] Local meteorological drivers (wind, temperature) affecting BC are underexplored.[42,43] To address these gaps, we conducted multi-site measurements across an urban–suburban transect in Chongqing to examine BC dynamics and their response to meteorology and emissions. Specifically, we aimed to: (1) identify temporal patterns of BC and its sources, (2) evaluate meteorological influences, and (3) assess co-pollutant correlations to refine source attribution.

BC can be termed as elemental carbon (EC), refractory black carbon (rBC), or equivalent black carbon (eBC), depending on the measurement method.[44] In this study, we refer to BC as eBC, which is calculated by converting the light absorption coefficient into mass concentration using a suitable mass absorption cross-section (MAC) applied by our measurement equipment. This study provides empirical insights into eBC behavior across urban–suburban areas under complex terrain and meteorology. The findings highlight the contrasting behaviors of black carbon components in response to emission types and meteorological conditions, revealing their distinct spatiotemporal signatures. These insights can support differentiated mitigation strategies, such as targeted control on vehicular emissions year-round, and seasonal restrictions on residential biomass combustion and port-related emissions. Overall, the study advances region-specific understanding of BC and offers policy-relevant insights for air quality and climate co-management.

2 Methods

2.1 Monitoring sites and collection periods

Field measurements were conducted from January to December 2024 at four sites (HJ, GY, JB, TJ) in metropolitan Chongqing (Fig. 1), classified as urban (HJ) or suburban (GY, JB, TJ) based on land use. HJ is located in central Chongqing, surrounded by dense traffic and residential areas. GY, JB, and TJ are located near the GuoYuan port, Jiangbei Airport, and TuanJie Railway freight station, respectively. These sites were deliberately selected to represent distinct source regimes—port/shipping (GY), airport (JB), rail freight (TJ), and dense urban traffic (HJ)—constituting a "spatial source separation" approach that enables a source-oriented comparison of BC concentrations across different urban microenvironments. Notably, the so-called "suburban" sites (GY, TJ, JB) are situated in peripheral zones where industrial and logistical facilities are concentrated—a direct consequence of stringent environmental policies that prohibit coal combustion and restrict high-emission activities within the Chongqing metropolitan core. While these locations reflect different local emission influences, they may not represent city-wide eBC levels. Establishing monitoring sites at cleaner background locations, better suited as regional reference points, is planned in future studies.

2.2 eBC measurement

eBC concentrations were measured using 7-wavelength aethalometers (Model-AE33, Magee Scientific), operating at 5 L min^{-1} with a $PM_{2.5}$ cyclones. Optical attenuation (ATN) and the absorption coefficient (b_{abs}) at 370–950 nm were calculated using assumed wavelength-dependent MAC values and a multiple-scattering correction factor (C_{ref}).[45] A dual-spot algorithm corrected filter-loading artifacts.[46] ATN at 880 nm was converted to eBC using MAC = 7.77 m^2 g^{-1} [44]. C_{ref} was set to 2.919, calculated as $C_0 \cdot H = 1.39 \times 2.1$, where C_0 is the manufacturer-recommended value for the "8060" filter tape in this study,[47] and H is a harmonization factor.[48,49]

2.3 Auxiliary measurements

All auxiliary measurements were conducted simultaneously with BC at each of the four sites. PM_{10} and $PM_{2.5}$ were measured using hybrid real-time monitors (5030i SHARP, Thermo Scientific). Gaseous pollutants (O_3, CO, SO_2, NO_2) were also monitored using Thermo analyzers (models 49i, 48i, 43i, 42i). Non-methane hydrocarbons (NMHCs) were quantified by an online GC-FID (EXPEC 2000). Meteorological data including relative humidity (RH), temperature (AT), pressure (AP), wind speed

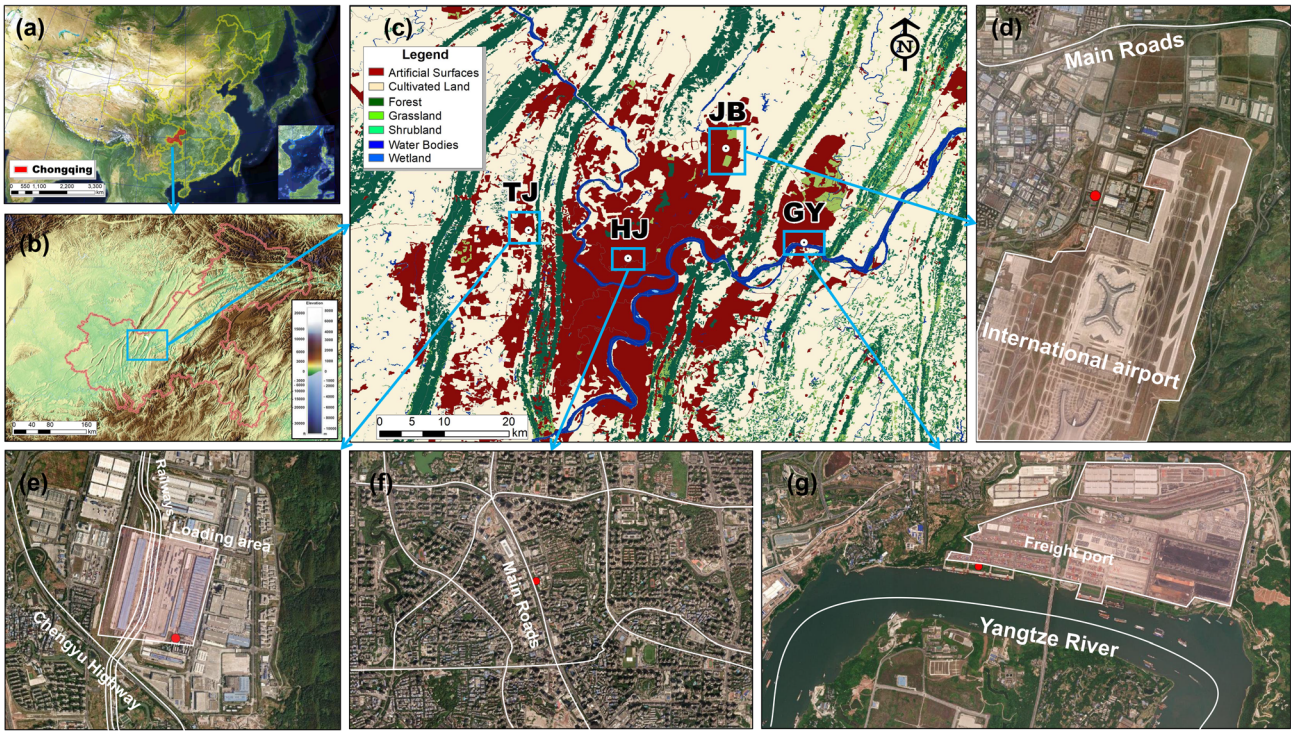

Fig. 1 Geographic distribution of the study area and sampling sites. (a) Location of Chongqing in China. (b) Topographic map of Sichuan Basin, Southwest China. (c) Land cover types in the central urban area of Chongqing based on GL30 data, with dark red areas indicating "artificial surfaces" (*i.e.*, surfaces resulting from human construction activities). (d)–(g) Satellite images of the surroundings of JB, TJ, HJ and GY site, respectively.

(WS), and wind direction (WD) were obtained from an automatic meteorological station (Lufft WS500, Hach).

2.4 Reanalysis and emission inventory

Hourly planetary boundary layer height (BLH) were retrieved from ERA5 reanalysis of European Centre for Medium-Range Weather Forecasts (ECMWF) at 0.25° resolution (https://doi.org/10.24381/cds.adbb2d47, accessed on: Jun 16, 2025). BC emission data were derived from the Global Emission Modeling System (GEMS),[50] covering global emissions of key pollutants (*e.g.*, CO_2, NO_x, SO_2, PM, BC, OC, PAHs) from 1960–2019 at 0.1° resolution (https://gems.sustech.edu.cn, accessed on: June 24, 2025). Given that the spatial distribution of global BC emission hotspots is generally stable over short timescales, the 2019 GEMS inventory remains representative for the present study. Gridded BC emissions from the Multi-resolution Emission Inventory for China (MEIC v2.0, https://meicmodel.org.cn, accessed on: May 9, 2026) at 0.25° × 0.25° resolution for the year 2023 were also used for regional-scale comparison in the SI (Fig. S15). Land cover data were obtained from GlobeLand30 (30 m resolution), developed by the National Geomatics Center of China (NGCC, https://www.webmap.cn/mapDataAction.do?method=globalLandCover; accessed on January 21, 2025), used to identify urban, vegetation, water, and other surface types.

2.5 Aethalometer model

The aethalometer model[51] apportions BC based on the wavelength dependence of light absorption. The b_{abs} is modeled as a sum of solid (*e.g.*, biomass, coal) and liquid fuel (*e.g.*, traffic-related) emissions following a power law: $b_{abs}(\lambda) \sim \lambda^{-AAE}$, where λ is wavelength and AAE is the Ångström exponent.[52,53] AAE values were set to 1 and 2 for liquid and solid fuels, respectively.[4,54–58]

AAE values from biomass and coal combustion are typically higher than those from traffic (excluding heavy fuel oil).[59–61] The original model assumes negligible coal combustion, allowing BC partitioning into fossil fuel and biomass burning sources.[47,62,63] However, coal consumption remains a major BC source in China,[64–66] especially in Beijing–Tianjin–Hebei region and southwest provinces.[67] BC source apportionment was therefore estimated as follow:

$$b_{abs}(470\ nm) = b_{abs}(470\ nm)_{liquid} + b_{abs}(470\ nm)_{solid} \quad (1)$$

$$b_{abs}(950\ nm) = b_{abs}(950\ nm)_{liquid} + b_{abs}(950\ nm)_{solid} \quad (2)$$

$$\frac{b_{abs}(470\ nm)_{liquid}}{b_{abs}(950\ nm)_{liquid}} = \left(\frac{470}{950}\right)^{-AAE_{liquid}} \quad (3)$$

$$\frac{b_{abs}(470\ nm)_{solid}}{b_{abs}(950\ nm)_{solid}} = \left(\frac{470}{950}\right)^{-AAE_{solid}} \quad (4)$$

$$BC_{liquid} = \frac{b_{abs}(950\ nm)_{liquid}}{b_{abs}(950\ nm)} \times BC(880\ nm) \quad (5)$$

$$BC_{solid} = BC(880\ nm) - BC_{liquid} \quad (6)$$

3 Results and discussion

3.1 Overview of eBC concentration

eBC concentrations varied modestly across the sites, with consistently higher levels at suburban locations. Annual averages followed the order: TJ ($3.04 \pm 2.07\ \mu g\ m^{-3}$) > GY ($2.95 \pm 1.79\ \mu g\ m^{-3}$) > JB ($2.49 \pm 1.62\ \mu g\ m^{-3}$) > HJ ($2.39 \pm 1.31\ \mu g\ m^{-3}$), consistent with observations in other megacities such as Los Angeles,[68] Madrid,[69] Milan,[70] Shanghai,[71] Beijing.[72,73] This trend reflects growing emissions in peri-urban areas amid reduced urban core pollution. As illustrated in Fig. 2, BC concentrations in Chinese cities are generally higher than those reported in Europe,[47,70,74,75] the United States,[68,76] and Japan,[77] but lower than those observed in India,[78,79] despite differences in observation periods and instrumentation.

Among Chinese cities, Chongqing exhibited slightly higher average eBC concentrations compared to southern coastal cities such as Shanghai, Shenzhen, and Guangzhou[71–73,80,81] (see Table S1 for additional comparisons). Notably, winter eBC at an urban site in 2016 reached 7.2 $\mu g\ m^{-3}$,[82] 2 to 3 times higher than current winter values ($3.2 \pm 4.7\ \mu g\ m^{-3}$), likely due to stricter air quality policies in recent years.[83]

The eBC_{liquid} concentrations (Fig. S1a) followed the order GY ≈ TJ > HJ > JB, while eBC_{solid} (Fig. S1b) was highest at TJ and JB and lowest at HJ. This demonstrates that liquid fossil fuel emissions dominate at all sites. The HJ site exhibited the highest proportion of liquid fuel ($83.6 \pm 6.2\%$) as shown in Fig. S1c, reflecting the significant influence of traffic emissions near roadways. Additionally, Fig. S2 showed that HJ had the highest levels of NMHC and NO_x, both of which are indicators of vehicular emissions.[84,85] Conversely, HJ recorded the lowest SO_2 concentration, while suburban sites exhibited considerably higher levels. These elevated concentrations underscore the substantial impact of coal or other heavy fuel combustion at these sites.[86,87] These contrasting urban–suburban patterns reflect the stringent emission controls enforced within the Chongqing metropolitan core (*e.g.*, coal ban, vehicle restrictions), which confine solid-fuel and industrial sources to peripheral zones.

The AAE also provides insight into aerosol sources. In this study, the AAE was derived by curve fitting a power function to the full spectral wavelength range. As depicted in Fig. S1d, the AAE value at the urban HJ site (1.19 ± 0.1) was notably lower than those at the suburban sites: JB (1.41 ± 0.2), TJ (1.35 ± 0.1), and GY (1.32 ± 0.2). A high AAE generally reflects an increased wavelength dependence of aerosol light absorption, indicating the presence of additional absorbing components beyond "pure" BC, particularly brown carbon (BrC) or aged organic matter.[88] Biomass burning typically produces high AAE values ranging from 1.2 to 2.9 due to BrC emissions under low

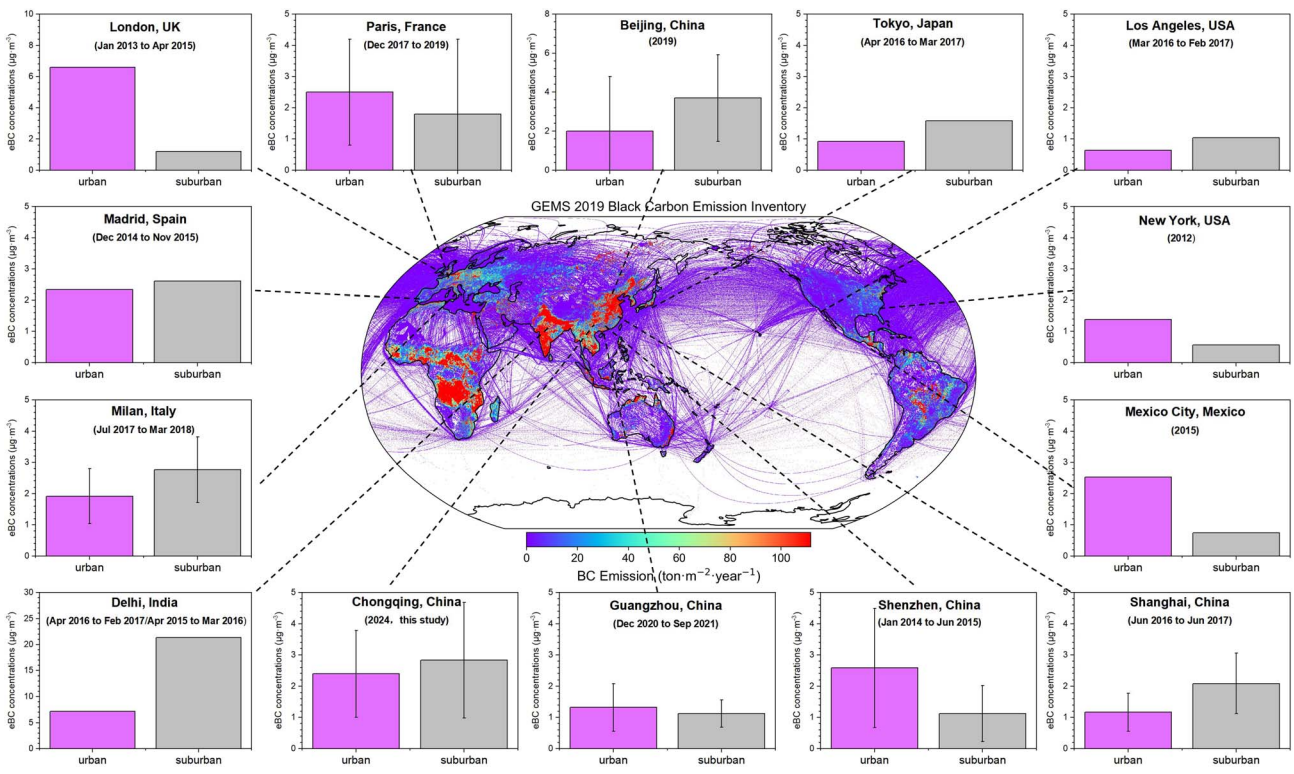

Fig. 2 BC concentrations in various megacities globally. The bar charts represent BC concentrations in both urban and suburban areas. The purple bars indicate concentrations in urban areas, while the grey bars represent suburban areas. The map in the center shows the global distribution of BC emissions from the GEMS inventory. Note that observation periods vary among the cited studies (see Table S1 for details).

combustion efficiency.[89–91] Residential coal combustion also contributes more organic carbon and BrC, resulting in higher AAE values ranging from 1.5 to 2.2.[60] In contrast, industrial combustion systems (*e.g.*, coal-fired power plants) operate at high efficiency and temperature, which removes much of the organic matter, yielding AAE values close to or even below 1. Furthermore, gasoline-fueled combustion typically emits "pure" BC with minimal BrC, leading to lower AAE values (0.8 to 1.3) compared to biomass or heavy fuel combustion.[59,60,92] The notably lower AAE at HJ is therefore fully consistent with the predominance of gasoline-fueled traffic emissions inferred from the eBC liquid fraction and trace gas profiles.

Beyond these site-averaged characteristics, the differences in AAE observed among the sites in this study are likely attributable to variations in dominant emission sources, which aligns with the source apportionment results from the aethalometer model. Interestingly, as shown in Fig. 3, the proportions of eBC_{liquid} and eBC_{solid} exhibited minimal variations when the eBC concentrations were low at the sites. However, as eBC concentrations increased, the trends in the proportions of eBC_{liquid} and eBC_{solid} became inconsistent. At the GY site, the proportion of eBC_{liquid} increased by 16% with rising eBC concentrations. At the TJ and JB sites, the proportions of eBC_{liquid} decreased by 19% and 8%, respectively, while eBC_{solid} accounted for nearly 50% at higher eBC concentrations. At the HJ site, the proportion of eBC_{liquid} remained relatively stable, fluctuating between 86% and 83%. This differential behavior suggests that the composition of emission sources at the sites varies under different eBC concentration levels, which is further supported by the changes in AAE shown in Fig. 3. At the GY site, the AAE rapidly decreased with increasing eBC concentration, approaching 1, suggesting a significant contribution from liquid fuel combustion emissions at higher BC levels—a pattern consistent with shipping emissions given the site's proximity to GuoYuan Port (see also Section 3.2.1 for cargo throughput analysis). At the HJ site, the hourly averaged AAE remained between 1.1 and 1.3 across all eBC concentration bins, with no systematic decrease during high-BC episodes. This indicates that the relative contribution of solid fuel combustion (*e.g.*, domestic heating) does not increase appreciably at this urban location, reinforcing the interpretation of a relatively stable influence from traffic-related emissions. The average AAE values at the TJ and JB sites were higher (ranging from 1.3 to 1.6), and a noticeable upward trend in AAE was observed as eBC concentrations increased. This suggests that these two sites are influenced by a combination of liquid and solid fuel combustion emissions. As eBC concentrations rise, the proportion of solid fuel emissions increases, which may be indicative of biomass burning or coal combustion emissions, prevalent in the Sichuan Basin during the autumn (SON) and winter (DJF) seasons.[93,94] In the subsequent sections, we will discuss the spatiotemporal characteristics of the changes in eBC_{liquid} and eBC_{solid} concentrations and the corresponding changes in emission source at each site.

3.2 Temporal characteristics

3.2.1 Monthly and seasonal variations. Further analysis of the daily averaged concentrations of eBC_{liquid} and eBC_{solid} at each site (Fig. 4) revealed that eBC_{liquid} concentrations ranged from 0.24 to 6.52 μg m^{-3},while eBC_{solid} concentrations ranged from 0.048 to 5.32 μg m^{-3}. Time series data show that eBC_{solid} concentrations tend to display stronger seasonal patterns across the various sites compared to eBC_{liquid}. This discrepancy is attributed to the fact that urban traffic flow exhibits less

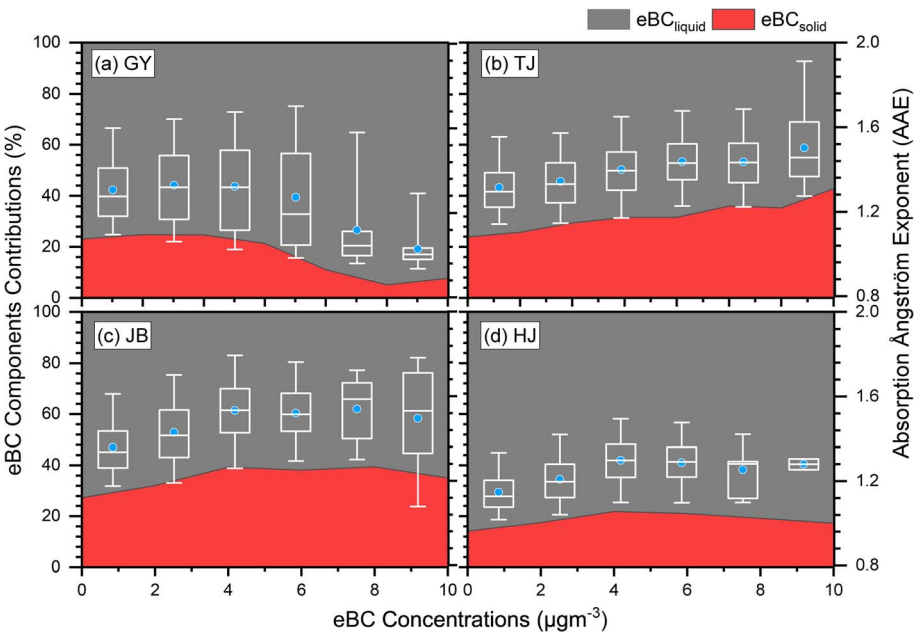

Fig. 3 Averaged contributions of eBC_{liquid} and eBC_{solid} as a function of eBC concentration, along with box (25th–75th percentile) and whisker (5th–95th percentile) plots of AAE at each site. (a) GY, (b) TJ, (c) JB, (d) HJ sites.

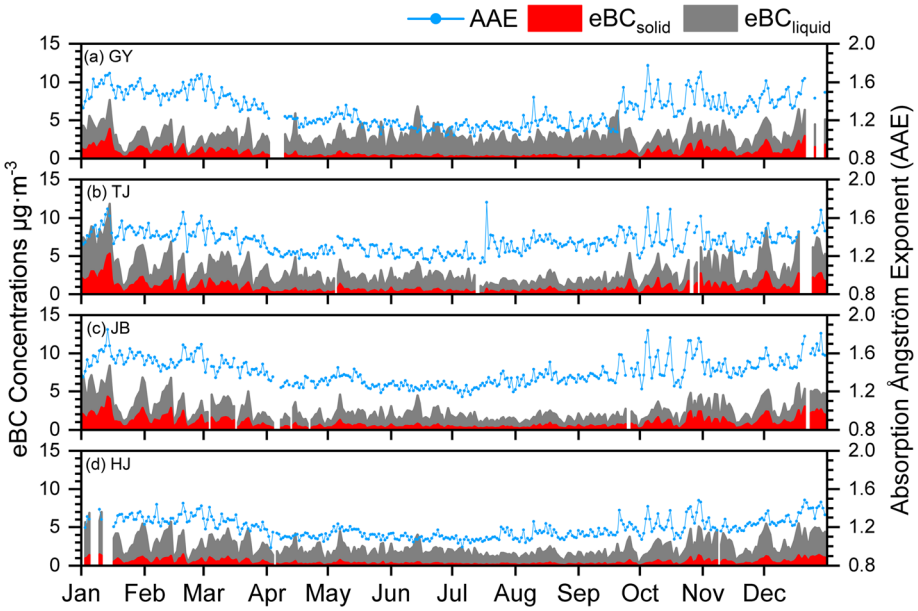

Fig. 4 Time series of eBC$_{liquid}$, eBC$_{solid}$, and AAE at each site. (a) GY, (b) TJ, (c) JB, (d) HJ sites.

seasonal variation than the seasonal emissions from solid fuel combustion (*e.g.*, domestic coal combustion and biomass burning), with the former being more prevalent at most sites.[47] Generally, aerosol concentrations (*e.g.*, $PM_{2.5}$ and BC) reached their highest levels during wintertime at most sites, as shown in Fig. S12a and b, primarily due to the seasonal variations in meteorological conditions (*e.g.*, lower BLH and WS) and emission sources (*e.g.*, domestic heating and meat fumigation).[23,29,95,96] The monthly variations of BLH and WS at each site are shown in Fig. S3. And the evidence for increased emission intensity from solid fuel combustion in autumn and winter is provided by our previous study.[94]

It is worth noting that, despite the relatively stable seasonal variations in eBC$_{liquid}$ across the sites, the contribution of eBC$_{liquid}$ at GY showed a notable increase from May to September 2024, as illustrated in Fig. 4a and S12d. During this period, concentrations were nearly 30% higher compared to the rest of the year. This seasonal enhancement is likely related to the site's proximity to the freight port in the city, where shipping activity on the Yangtze River typically intensifies during the flood season. As shipping companies schedule more voyages to take advantage of elevated water levels and improved navigability, the observed increase in eBC$_{liquid}$ may be attributed to enhanced emissions from inland waterway transport. In fact, this increase in activity is supported by the recent cargo throughput data for Chongqing Guoyuan Port (Table S2), which further demonstrates the elevated port activities during the flood season. In contrast, shipping volume generally declines during the dry season, potentially leading to lower contributions outside the flood period.[97,98] Moreover, Fig. S12e showed that the proportion of eBC$_{liquid}$ at the HJ site consistently remained above 75%, indicating a strong influence from vehicular emissions based on its monthly variation. Meanwhile, at suburban sites (GY, JB, and TJ), the contribution of eBC$_{liquid}$ decreased from approximately 80% in spring (MAM) and summer (JJA) to around 60% in autumn and winter. This decline can be attributed to enhanced seasonal emission sources, such as coal and wood burning for domestic heating, as well as the traditional meat fumigatetion (*e.g.*, sausage and bacon) in Southwest China, as mentioned earlier.

Another point to note is that the monthly average AAE at the urban HJ site exhibited a relatively narrow fluctuations, primarily between 1.1 and 1.3, indicating a dominant influence from vehicular emissions. In comparison, suburban sites (GY, JB, and TJ) exhibited greater variability in AAE, ranging from 1.1 to 1.6, suggesting the presence of additional sources (*i.e.*, solid fuel combustion) during winter. Overall, AAE demonstrated a pronounced seasonal pattern, with lower values in spring and summer and higher values in autumn and winter. This seasonal trend is likely driven by both changes in emission sources and meteorological conditions, particularly reduced atmospheric dispersion and frequent stagnation events in autumn and winter, which facilitate the aerosols aging. Aged aerosols typically exhibit higher AAE values, as indicated by several studies.[99,100]

3.2.2 Diurnal patterns and weekend effect. Diurnal plots (Fig. 5) were used to validate whether the temporal variation patterns of the two eBC components aligned with the expected behavior of their respective emission sources. In general, the diurnal variation of aerosol pollutants (*e.g.*, BC) is primarily driven by atmospheric dispersion conditions (*e.g.*, BLH and WS), with a typical pattern of lower concentrations during the daytime and higher concentrations at nighttime. At the urban site HJ, eBC$_{liquid}$ displayed a distinct morning peak at 07:00 (local time, LT), associated with rush hour emissions, followed by a decline as BLH increased. Subsequently, a smaller peak emerged around 20:00 LT, coinciding with reduced atmospheric mixing and enhanced surface accumulation in the

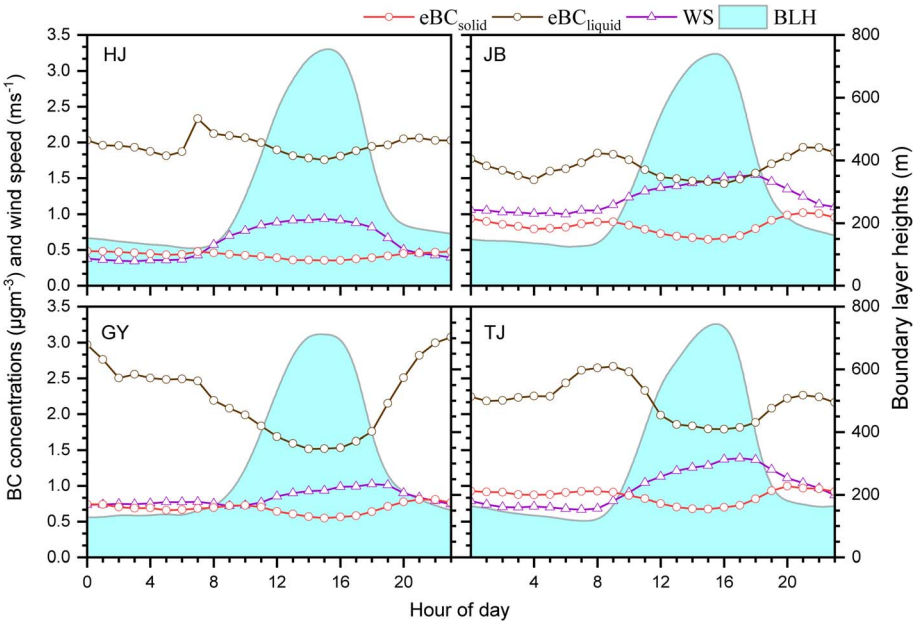

Fig. 5 Mean hourly variations in eBC$_{liquid}$ and eBC$_{solid}$, as well as meteorological parameters (WS and BLH) across the sites.

evening. As illustrated in Fig. S4a, the eBC$_{liquid}$ at HJ exhibited a pattern similar to NO_x, indicating the prevailing influence of vehicular emissions. This bimodal distribution was also observed at JB and TJ. The first peak typically occurred prior to the development of the boundary layer and was attributed to the accumulation of traffic-related emissions under stagnant conditions. As BLH deepened and WS strengthened, enhanced vertical and horizontal dispersion led to a reduction in eBC$_{liquid}$ concentrations. The evening rebound coincided with weakened atmospheric mixing. In contrast, eBC$_{solid}$ variations were more strongly influenced by dispersion than by source activity. Its levels remained stable before BLH growth and declined notably as daytime mixing intensified.

Notably, eBC$_{liquid}$ at the GY site exhibited a distinct nighttime unimodal pattern. As discussed in Section 3.2.1, port activities near the GY site intensify during the flood season (May–September), resulting in elevated eBC$_{liquid}$ concentrations. This suggests that the observed nighttime peak is closely linked to port-related operations. A study using VIIRS satellite nighttime light data across 601 global anchorages demonstrated substantial nocturnal port activity, particularly during high-volume shipping periods.[101] Similarly, Murata[102] employed CE-SAT-IIB nighttime satellite imagery to assess operations at multiple terminals in Tokyo Port, revealing elevated nighttime activity during high-demand shipping periods. In addition, long-term noise monitoring outside ports has also confirmed frequent night operations, especially during peak periods.[103]

Previous studies[33,55,75,104] have reported a "weekend effect" in carbonaceous aerosols, primarily attributed to variations in anthropogenic emissions between weekdays and weekends. To further evaluate the consistency between the expected behavior of eBC emissions and the observed spatiotemporal variation patterns, we analyzed the diurnal variations in eBC concentrations across all sites for each day of the week (Fig. 6).

At HJ, the weekday morning peak of eBC$_{liquid}$ disappeared on weekends, and the evening peak was notably reduced, indicating a significant decline in local traffic-related activities during weekends. Unlike HJ, located in a typical urban center and sensitive to commuter-related traffic changes, the JB and TJ sites are adjacent to an airport and a railway freight station, respectively. As a result, although the bimodal patterns of eBC$_{liquid}$ at JB and TJ were also attenuated on weekends, the decrease was less pronounced. This difference indicates that transportation activities around JB and TJ are less sensitive to the weekday/weekend differences due to continuous traffic flows, thus reducing the weekend effect. At the GY site, nighttime freight operations at the nearby port remain the dominant factor influencing eBC$_{liquid}$ concentrations. While elevated concentrations were observed throughout the week, Fig. 6c reveals a reduction in nighttime levels from Saturday night to Sunday daytime, implying a temporary decline in port activity. However, this decrease was not statistically significant, as confirmed by the *t*-test results presented later.

For eBC$_{solid}$, no evident fluctuations between weekdays and weekends were observed across sites, suggesting that its emission sources (*e.g.*, biomass burning, residential coal combustion) remained relatively stable throughout the week. This limited temporal variability contrasts with the more pronounced fluctuations in eBC$_{liquid}$, highlighting the distinct responses of the two components to temporal changes. Consistent with this, previous studies[105,106] reported similar negligible weekday/weekend differences at sites near industrial areas or rural suburbs.

Additionally, an independent samples *t*-test was conducted to asess the "weekend effect" (Fig. S5). Statistically significant differences in eBC$_{liquid}$ were found at the HJ ($p < 0.0001$), JB ($p < 0.01$), and TJ ($p < 0.01$) sites, whereas no significant difference was detected at the GY site. Although a reduction in nighttime

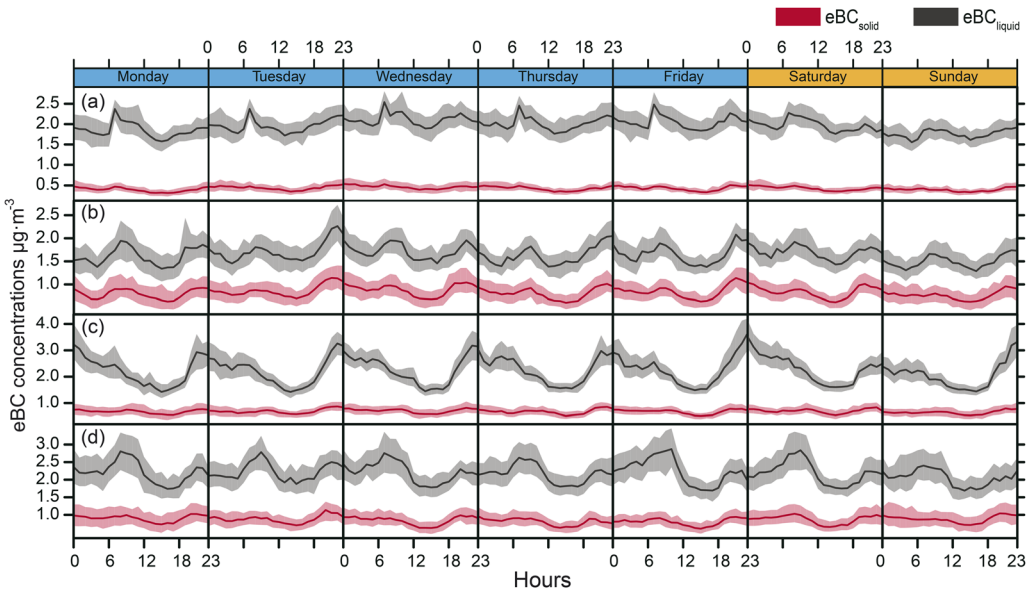

Fig. 6 Mean hourly variations in eBC_{liquid} and eBC_{solid} for each day of the week across the sites. (a) HJ, (b) JB, (c) GY, (d) TJ sites.

eBC_{liquid} was observed at GY, it did not reach the 0.01 significance level, indicating that the "weekend effect" at GY was not pronounced enough. No statistically significant differences in eBC_{solid} were detected at any of the sites at the 0.01 significance level.

3.3 Wind dependence of eBC concentrations

Wind rose plots (Fig. S6) indicated that hourly wind speeds were generally low across all sites, with suburban locations experiencing slightly higher values than the urban site. The hourly average WS followed the order: JB (1.3 ± 0.8 m s^{-1}) > TJ (1.0 ± 0.8 m s^{-1}) > GY (0.9 ± 0.4 m s^{-1}) > HJ (0.6 ± 0.4 m s^{-1}). The overall low WS are consistent with the weak ventilation typical of Chongqing's complex terrain,[26] while the lower values at the urban site likely reflect enhanced surface roughness from dense buildings and street canyons.[107] However, WD showed significant variability, suggesting that the spatial heterogeneity of emission sources influences site-specific eBC concentrations. To identify local BC sources, bivariate polar plots[108,109] were employed. As shown in Fig. 7a, high eBC concentrations generally occurred under low WS (<1 m s^{-1}), implying a dominant role of local sources and poor dispersion.

At HJ, high eBC_{liquid} concentrations were linked to southern and northern winds, aligning with nearby traffic routes, while eBC_{solid} peaked under northeasterly winds. Despite these directional preferences, the two components showed minor

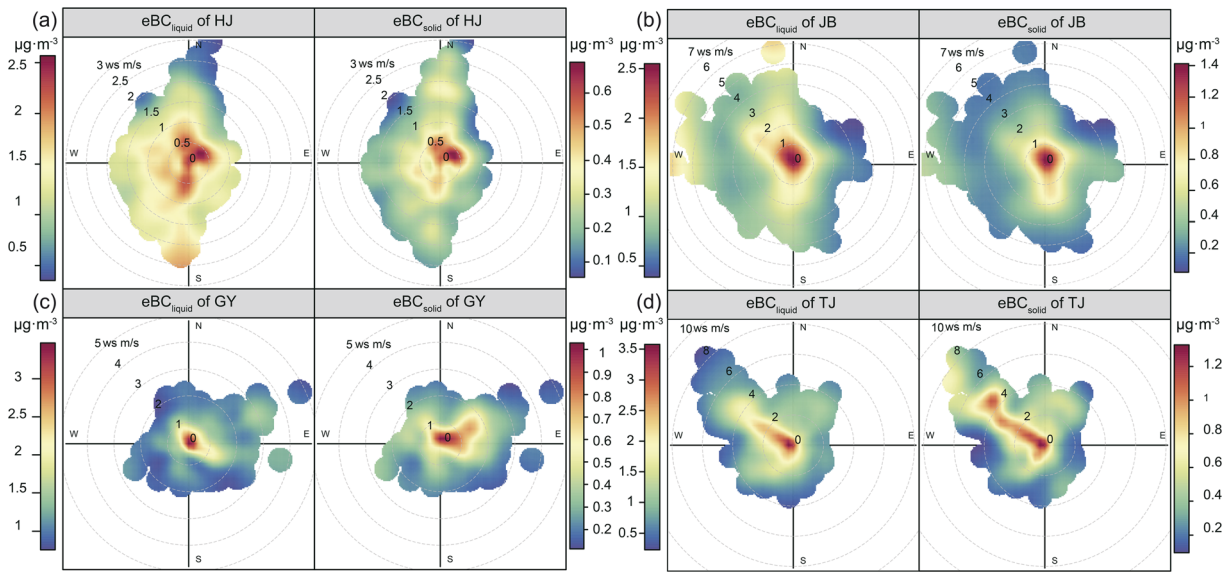

Fig. 7 Polar plots of eBC_{liquid} and eBC_{solid} for the sites (a) HJ, (b) JB, (c) GY, and (d) TJ.

differences in WD, indicating well-mixed pollution. Seasonal variability was limited but followed a slight north–south gradient (Fig. S7a and b). To further investigate the variability in emission sources, we established pairwise robust regression surface relationships[110] between eBC_{liquid} and eBC, and between eBC_{solid} and eBC. Fig. 8a reveals that under southerly and southwesterly winds, nearly all eBC is present in the form of eBC_{liquid}, with a proportion approaching 0.8, primarily due to traffic emissions. Easterly winds showed significant variability, indicating regional contributions from biomass or coal combustion. Seasonal variations in the robust slopes (Fig. S8a and b) confirmed persistent traffic contributions under westerly and southwesterly winds, with values remaining between 0.75 and 0.9. Meanwhile, eBC_{solid} emissions from northerly winds occurred mainly in autumn and winter, as discussed in Section 3.2.1, suggesting that solid fuel combustion sources from the north can still impact the central urban area during specific periods.

At JB, high eBC concentrations were predominantly observed under calm northerly winds. While directional differences between eBC_{liquid} and eBC_{solid} were minor, regression slopes (Fig. 8b) revealed spatial heterogeneity: eBC_{liquid} dominated westward (traffic), whereas eBC_{solid} peaked east and south, likely due to biomass burning or residential coal use. The southeastern sector of JB is influenced by airport emissions, where aviation fuels with high sulfur content are used. Such fuels can produce aerosols with elevated AAE values.[60] In addition, low-temperature combustion during aircraft ground operations has been reported to yield AAE values >3.5.[111,112] These high-AAE aerosols may thus cause systematic overestimation of eBC_{solid} when applying the aethalometer model in this region.

At TJ, eBC was strongly WD-dependent. Both eBC_{liquid} and eBC_{solid} peaked under NW winds, with eBC_{solid} rising at higher WD, likely from a nearby freight yard. eBC_{liquid} dominated at WD < 6 m s^{-1} (proportion > 0.65), while eBC_{solid} prevailed at higher WD (Fig. 8c), suggesting distinct source regimes. Fig. S8 showed high eBC_{solid} under strong NW winds in autumn and spring, coinciding with regional biomass burning peaks.[30,94]

At GY, spatial patterns diverged: eBC_{liquid} was higher in the SE, eBC_{solid} in the NE. Summer eBC_{liquid} peaks occurred under low WD (Fig. S8), likely from nearby port operations which discussed in Section 3.2.2. Notably, the site uniquely showed a summer annual maximum, emphasizing port activity's role. Meanwhile, eBC_{solid} peaked in winter from the north, similar to other sites. Robust regression (Fig. 8d) confirmed distinct source zones: SE (port) for eBC_{liquid}, NE (biomass/coal) for eBC_{solid}.

Extending this wind-dependent analysis to AAE (Fig. S13 and S14) reveals additional site-specific features: at JB and GY, AAE decreases with increasing wind speed, consistent with the dilution of local solid fuel sources. In contrast, higher wind speeds at TJ and HJ are accompanied by elevated AAE, pointing to the transport of solid-fuel-rich or aged aerosols from upwind regions,[99] which further corroborates the source influences identified above.

A comparison of gridded BC emission inventories over the study region is provided in Fig. S15. According to both the GEMS and MEIC inventories,[113] TJ, JB, and HJ are located within or immediately adjacent to high-BC-emission grid cells, consistent with the elevated eBC concentrations at these sites. The GY site, by contrast, falls near the edge of the high-emission zone in both inventories. This likely reflects the limited spatial resolution of current publicly available inventories, as well as the fact that the GuoYuan Port was still under construction when the GEMS 2019 inventory was compiled (the port was not fully completed until 2022). The MEIC 2023 inventory, although more recent, has a coarser resolution that may also not fully

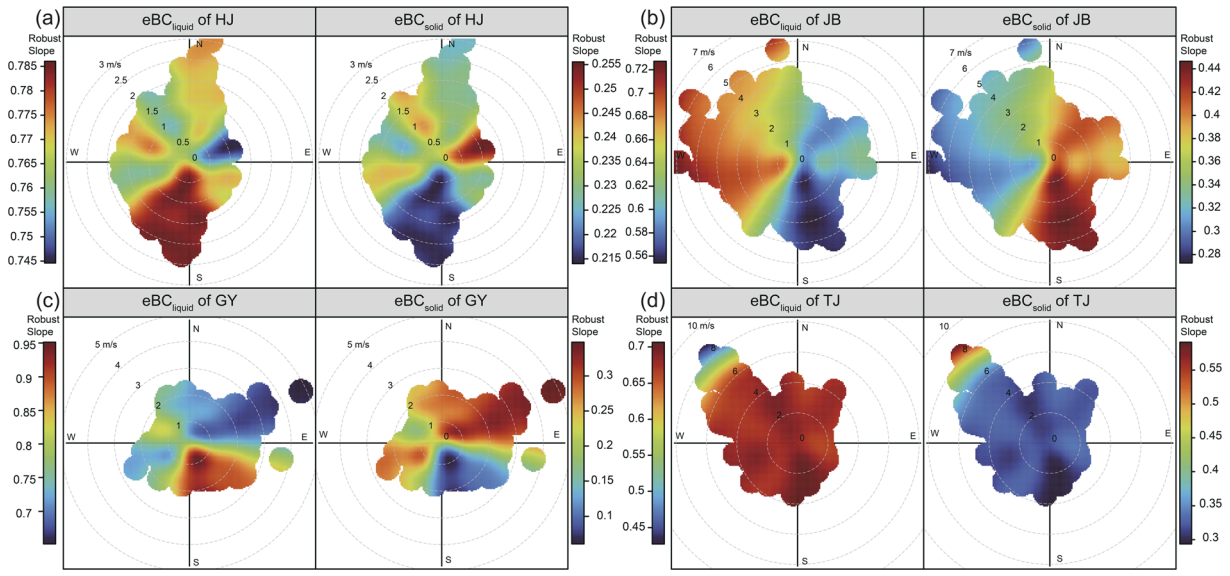

Fig. 8 Polar plots of the robust regression slope between eBC_{liquid} and eBC, and between eBC_{solid} and eBC, using pairwise statistics, at (a) HJ, (b) JB, (c) GY, and (d) TJ.

resolve localized shipping emissions. This comparison underscores the complementary value of ground-level monitoring in characterizing emissions from rapidly evolving, seasonally modulated sources that gridded inventories may overlook.

3.4 Relationships between the pollutants

Pollutant relationships at each site were evaluated using Spearman correlation matrics with hierarchical clustering (Fig. 9). $PM_{2.5}$ showed strong positive correlations ($R_s > 0.7$) with both eBC_{solid} and eBC_{liquid} at most sites, except GY, where eBC_{liquid} had a lower correlation ($R_s = 0.43$). This indicates eBC concentrations increased concurrently with elevated regional aerosol pollution, aligning with previous studies.[10,114–116] While both eBC components rose with $PM_{2.5}$ at most sites (Fig. S9), eBC_{liquid} at GY lacked a clear upward trend—likely due to intensified port activity during the flood season (Fig. 4 and S12d). Additionally, as $PM_{2.5}$ pollution worsened, both AAE and the fraction of eBC_{solid} increased. This reflects seasonal enhancement of emission sources, particularly from residential coal and biomass burning during autumn and winter, as reported by Zhang[67] and Mousavi[68] also reflects aerosol aging, which increases AAE through enhanced long-wavelength absorption.[99,100]

eBC_{liquid} showed strong correlations with NMHC across sites, especially at TJ and HJ, indicating a strong gasoline combustion influence. The weaker correlation at JB may be attributed to its distance from major roads (>1 km) and the high reactivity of NMHC.[117,118] Additionally, eBC_{liquid} showed strong correlations with NO_x at all sites, underscoring the impact of traffic-related emissions. However, at HJ, despite the highest NO_x levels (Fig. S2), its correlation with eBC_{liquid} was weakest ($R_s = 0.43$). This may be due to complex urban emissions and enhanced photochemistry, where NO and O_3 participate in a reversible equilibrium,[119] making NO_x an ambiguous indicator of primary sources. eBC_{solid} showed stronger correlations with SO_2 and AAE, indicating contributions from high-sulfur-content fuel like coal and heavy fuel oil.[60,92] Biomass burning could not be fully assessed due to the lack of specific tracers (*e.g.*, K^+, levoglucosan), but its typical high-AAE signature[111] may partially explain the observed enhancement in AAE and its association with eBC_{solid}. This highlights the need for future measurements—including ions, inorganic elements, and organic molecular markers—to better characterize source processes and distinguish the optical properties of specific emission sources in this region. The spatial source separation framework established in this study can inform the selection of

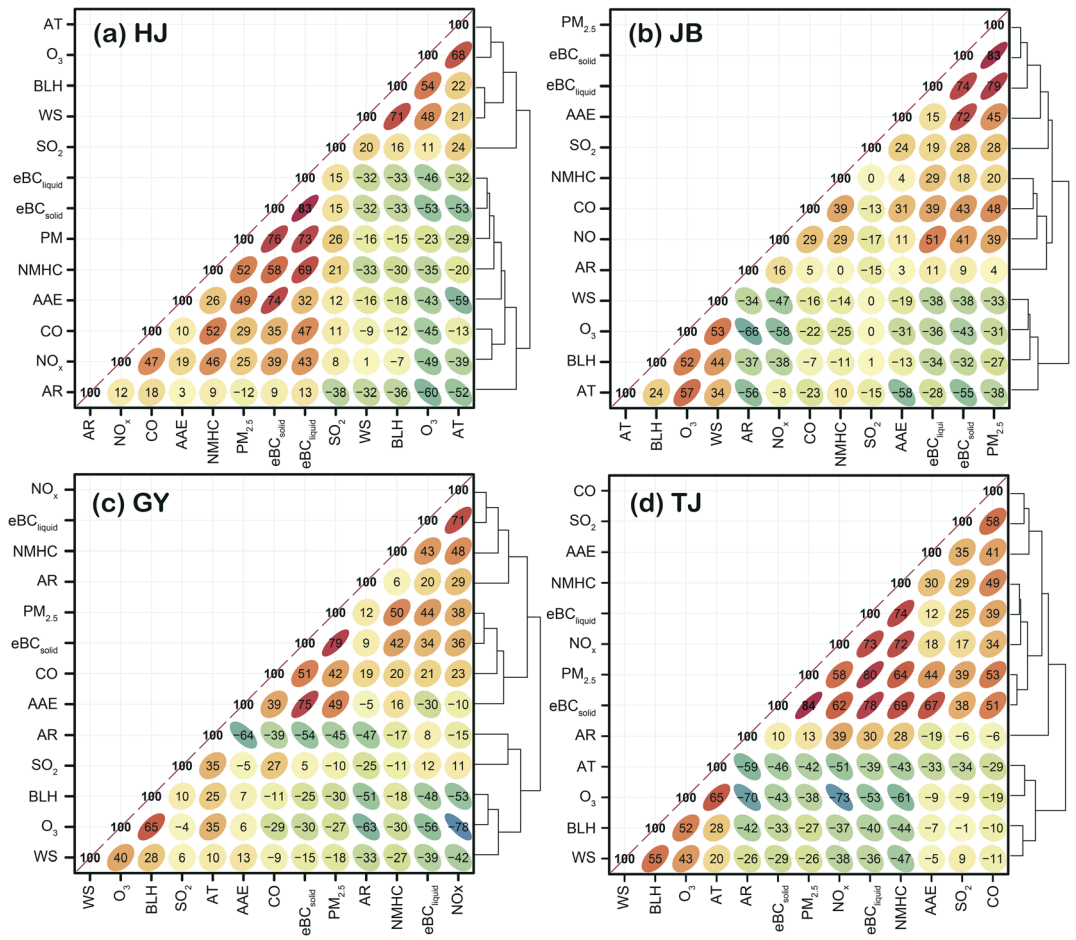

Fig. 9 Correlation matrixs between the pollutants at each site. (a) HJ, (b) JB, (c) GY, (d) TJ sites.

tracer species and receptor sites for formal PMF/CMB analyses in such future campaigns.

Ambient temperature (AT) was inversely correlated with eBC, especially eBC_{solid}, reflecting increased heating-related emissions under lower temperatures.[60,89] However, this trend was absent at GY, likely due to high summer eBC_{liquid} from port activity. As shown in Fig. S10 and S11, eBC_{solid} concentrations peaked within the 8 to 18 °C range. While JB, TJ, and HJ also exhibited elevated eBC_{liquid} levels in this range, their temperature sensitivity was comparatively weak. In contrast, the eBC_{liquid} at GY site peaked at 24 to 36 °C. Fig. S11 further reveals that at GY, JB, and HJ, eBC_{solid} was more prevalent under lower temperatures, while eBC_{liquid} increased with higher temperatures. However, at TJ, no clear temperature dependence was observed, likely due to steady industrial/solid fuel emissions,[105] unlike the more seasonally driven patterns at other sites.[96]

To further assess the seasonal stability of these pollutant relationships, the Spearman correlation analysis was repeated for each meteorological season at each site (Fig. S16–S19). Several seasonal patterns emerged consistently. First, correlations involving eBC_{solid}, particularly those with SO_2, AAE, and AT, were strongest in autumn and winter, reflecting enhanced solid fuel combustion and biomass burning during colder months. Second, eBC_{liquid} correlations with NMHC remained strong and stable year-round at all sites, consistent with the persistent contribution of traffic emissions. Third, the GY site exhibited a notable seasonal departure: the eBC_{liquid}–AAE correlation shifted from strongly negative in summer ($R_s \approx -0.60$) to positive in winter ($R_s \approx 0.40$), capturing the transition from shipping-dominated emissions during the flood season to a mixed influence of solid fuel combustion in winter. Similarly, the eBC_{liquid}–$PM_{2.5}$ correlation at GY weakened substantially in summer, consistent with the decoupling of port-related emissions from the regional aerosol background. These seasonal correlation patterns, consistent with the source-specific temporal variations discussed in Sections 3.2 and 3.3, indicate that the relationships among pollutants are not entirely stable across seasons; rather, they vary meaningfully with season and source activity.

3.5 Uncertainties of the aethalometer source apportionment

Several sources of uncertainty should be considered when interpreting the aethalometer-derived source apportionment results. First, the model assumes fixed AAE values for liquid (AAE ≈ 1) and solid (AAE ≈ 2) fuel combustion. While these values are widely adopted in the literature,[59,60] the actual AAE of specific sources can deviate due to differences in fuel composition, combustion conditions, and atmospheric aging. The reported source contributions should therefore be regarded as semi-quantitative estimates. A systematic sensitivity analysis—varying the assumed AAE values within plausible ranges—would help quantify the impact of this uncertainty on the apportioned contributions and represents a useful direction for future refinement of these results. Second, aerosol aging can increase AAE through enhanced long-wavelength absorption,[99,100] potentially leading to an overestimation of the solid fuel fraction for aged aerosols. This may partially explain the elevated AAE observed at the HJ site under higher wind speeds (Fig. S13). Third, the two-component model cannot resolve subcategories within each fuel type (*e.g.*, biomass burning *vs.* residential coal, or traffic *vs.* shipping). At JB, the influence of airport emissions with potentially high AAE values[111,112] introduces additional uncertainty in the eBC_{solid} estimates. Despite these limitations, the consistency between the aethalometer results and independent tracers (NMHC, NO_x, SO_2, Fig. S2 and 9), the physically interpretable seasonal and diurnal patterns (Fig. 4–6), and the site-specific differences that align with known source distributions (Fig. 7 and 8), collectively support the robustness of the main conclusions drawn from this analysis.

4 Conclusions

This study systematically characterized the spatiotemporal patterns and source contributions of eBC and its combustion components across an urban–suburban gradient in Chongqing, a megacity in a mountainous basin. A deliberate "spatial source separation" monitoring design, in which sites were selected to represent distinct emission regimes (port, airport, rail freight, and dense urban traffic), enabled a source-oriented assessment of BC pollution in this complex terrain.

Annual mean eBC concentrations ranged from 2.38 to 3.04 μg m^{-3}, with slightly higher levels in suburban areas. This urban–suburban contrast reflects the combined effect of stringent emission controls within the metropolitan core—which confine coal combustion and high-emission industrial activities to peripheral zones—and the proximity of suburban sites to major logistical and industrial sources. Winter peaks were mainly driven by residential heating and unfavorable meteorological conditions, reflecting the sensitivity of BC pollution to seasonal energy demand and climate-related meteorological extremes.

Source apportionment based on AAE diagnostics indicated that liquid fuel combustion (*e.g.*, traffic) dominated eBC, particularly in urban areas (up to 83.6%), while solid fuel combustion (*e.g.*, biomass, coal) contributed more in suburban regions during autumn and winter, highlighting the importance of promoting clean energy transitions in peri-urban areas. Diurnal and weekly trends of eBC_{liquid} reflected traffic and port activity influences at HJ and GY, respectively. A seasonal reversal in the eBC_{liquid}–AAE relationship at GY—from strongly negative in summer to positive in winter—further captured the transition from shipping-dominated emissions during the flood season to a mixed influence of solid fuel combustion in winter. In contrast, eBC_{solid} exhibited stronger seasonal variation, reflecting episodic combustion. These findings highlight that seasonal river freight activity can significantly enhance BC levels, suggesting the need to consider shipping-related emissions in regional air quality management. A significant weekend decline in eBC_{liquid} further confirmed its traffic origin, while eBC_{solid} remained unaffected.

Correlation analysis with gaseous pollutants and meteorological parameters differentiated source types: eBC_{liquid} was

strongly associated with NO_x and NMHCs, while eBC_{solid} correlated with SO_2 and AAE, suggesting high-sulfur fuel combustion. Seasonally resolved correlation matrices further revealed that while certain source–tracer pairs (*e.g.*, eBC_{liquid}–NMHC) remained stable year-round, others varied meaningfully with season—underlining the value of time-resolved analysis in assessing tracer reliability. Negative correlations with temperature supported heating-related contributions. Wind analysis showed that cold, stagnant conditions promoted eBC accumulation, with source regions varying by site and season, underscoring how terrain–meteorology interactions may intensify air pollution episodes under climate variability. A comparison with gridded emission inventories (GEMS and MEIC) confirmed that the sites generally lie within high BC emission zones, while also highlighting that current inventories do not fully resolve localized, seasonally modulated sources such as port operations—demonstrating the complementary value of ground-level monitoring.

The contrasting behaviors of eBC_{liquid} and eBC_{solid} highlight the value of component-resolved BC analysis in identifying source-specific impacts and related health risks. The spatial source separation framework demonstrated here provides a practical and transferable monitoring strategy for other complex urban environments seeking to evaluate the influence of specific emission sources with relatively modest instrumentation. Our findings emphasize the need for year-round traffic emission control, alongside seasonal restrictions on shipping and biomass burning. These results provide a basis for targeted air quality strategies in complex urban–suburban settings, with implications for rapidly urbanizing regions globally.

Conflicts of interest

There are no conflicts to declare.

Data availability

The datasets supporting the conclusions of this article are available at the Mendeley Data repository through https://doi.org/10.17632/dkh855f28z.1. Data includes daily averaged concentrations of equivalent black carbon (eBC) and its source-apportioned fractions (eBC_{liquid} from fossil fuel, eBC_{solid} from biomass/coal), co-pollutants (NO_x, SO_2, NMHCs), and key meteorological parameters (temperature, wind speed) for one urban and one suburban site in Chongqing, China, covering the experiment period. Due to data use agreements with the Chongqing Municipal Bureau of Ecology and Environment, the underlying high-frequency (*e.g.*, 1 minute) raw instrument data are not publicly shared. The datasets deposited in Mendeley data are sufficient to reproduce all the figures and statistical analyses presented in this article.

Supplementary information (SI): two tables and nineteen figures. Table S1 provides a global comparison of black carbon concentrations in megacities. Table S2 provides GuoYuan Port cargo throughput data. Fig. S1–S19 present detailed supplementary statistical analyses including box plots, polar plots, wind roses, scatter plots, and seasonal correlation matrices of eBC components, co-pollutants, meteorological parameters, and emission comparisons across all study sites. See DOI: https://doi.org/10.1039/d6ea00019c.

Acknowledgements

This study was funded by the National Key Research and Development Program of China (No. 2023YFC3709303 and No. 2023YFC3709302), the Chongqing Key Projects for Technological Innovation and Application Development (No. CSTB2022TIAD-CUX0008), and the Environmental Monitoring Scientific Research Development Fund of Chongqing Ecological Environment Monitoring Center (No. CQHJ-NBKY-2023-001). We gratefully acknowledge the ECMWF, NGCC, and SUSTech for providing the ERA5 dataset, GL30 dataset, and GEMS emission inventory data used in this study. We would like to express our sincere gratitude to David Carslaw (University of York) and Stuart Grange (Queensland University of Technology) for developing the "openair" package in R, which was essential to this study. We would also like to thank Cheng Wu at Jinan University for generously providing the open-source software for graphic drawing. We also thank Xiao Han (Institute of Atmospheric Physics, Chinese Academy of Sciences) for helpful discussions on emission inventory data, and Yanyun He (Magee Scientific) for expert advice on AE33 instrument uncertainties.

References

1 T. C. Bond, S. J. Doherty, D. W. Fahey, P. M. Forster, T. Berntsen, B. J. DeAngelo, M. G. Flanner, S. Ghan, B. Kärcher, D. Koch, S. Kinne, Y. Kondo, P. K. Quinn, M. C. Sarofim, M. G. Schultz, M. Schulz, C. Venkataraman, H. Zhang, S. Zhang, N. Bellouin, S. K. Guttikunda, P. K. Hopke, M. Z. Jacobson, J. W. Kaiser, Z. Klimont, U. Lohmann, J. P. Schwarz, D. Shindell, T. Storelvmo, S. G. Warren and C. S. Zender, Bounding the role of black carbon in the climate system: A scientific assessment, *J. Geophys. Res.:Atmos.*, 2013, **118**, 5380–5552.

2 J. T. Everett, A Review of Progress in Constraining Global Black Carbon Climate Effects, *Earth Syst. Environ.*, 2022, **6**, 771–785.

3 V. Ramanathan and G. Carmichael, Global and regional climate changes due to black carbon, *Nat. Geosci.*, 2008, **1**, 221–227.

4 K. Cheng, Y. Zhong, X. Li, S. Li, M. Ayitken, W. Zhang and X. Liu, Assessment of pollution sources and health risks of black carbon aerosols in industrial cities of Northwestern China using light absorption observations, *Atmos. Pollut. Res.*, 2025, **16**, 102381.

5 X. Zhu, B. Liu, C. Guo, Z. Li, M. Cheng, X. Zhu and Y. Wei, Short and long-term association of exposure to ambient black carbon with all-cause and cause-specific mortality: A systematic review and meta-analysis, *Environ. Pollut.*, 2023, **324**, 121086.

6 A. J. Ding, X. Huang, W. Nie, J. N. Sun, V.-M. Kerminen, T. Petäjä, H. Su, Y. F. Cheng, X.-Q. Yang, M. H. Wang,

X. G. Chi, J. P. Wang, A. Virkkula, W. D. Guo, J. Yuan, S. Y. Wang, R. J. Zhang, Y. F. Wu, Y. Song, T. Zhu, S. Zilitinkevich, M. Kulmala and C. B. Fu, Enhanced haze pollution by black carbon in megacities in China, *Geophys. Res. Lett.*, 2016, **43**, 2873–2879.

7 Z. Wang, X. Huang and A. Ding, Dome effect of black carbon and its key influencing factors: a one-dimensional modelling study, *Atmos. Chem. Phys.*, 2018, **18**, 2821–2834.

8 S. Cui, D. Huang, Y. Wu, J. Wang, F. Shen, J. Xian, Y. Zhang, H. Wang, C. Huang, H. Liao and X. Ge, Chemical properties, sources and size-resolved hygroscopicity of submicron black-carbon-containing aerosols in urban Shanghai, *Atmos. Chem. Phys.*, 2022, **22**, 8073–8096.

9 A. Sedlacek, E. Lewis, T. Onasch, P. Zuidema, J. Redemann, D. Jaffe and L. Kleinman, Using the Black Carbon Particle Mixing State to Characterize the Lifecycle of Biomass Burning Aerosols, *Environ. Sci. Technol.*, 2022, **56**, 14315–14325.

10 H. Zheng, S. Kong, F. Wu, Y. Cheng, Z. Niu, S. Zheng, G. Yang, L. Yao, Q. Yan, J. Wu, M. Zheng, N. Chen, K. Xu, Y. Yan, D. Liu, D. Zhao, T. Zhao, Y. Bai, S. Li and S. Qi, Intra-regional transport of black carbon between the south edge of the North China Plain and central China during winter haze episodes, *Atmos. Chem. Phys.*, 2019, **19**, 4499–4516.

11 WHO, *Health Effects of Black Carbon*, World Health Organization, Regional Office for Europe, Copenhagen, 2012.

12 CCAC, Black Carbon, *Black Carbon, Climate and Clean Air Coalition*, Paris, 2024.

13 R. M. Hoesly, S. J. Smith, L. Feng, Z. Klimont, G. Janssens-Maenhout, T. Pitkanen, J. J. Seibert, L. Vu, R. J. Andres, R. M. Bolt, T. C. Bond, L. Dawidowski, N. Kholod, J. Kurokawa, M. Li, L. Liu, Z. Lu, M. C. P. Moura, P. R. O'Rourke and Q. Zhang, Historical (1750–2014) anthropogenic emissions of reactive gases and aerosols from the Community Emissions Data System (CEDS), *Geosci. Model Dev.*, 2018, **11**, 369–408.

14 Y. Qin and S. D. Xie, Spatial and temporal variation of anthropogenic black carbon emissions in China for the period 1980–2009, *Atmos. Chem. Phys.*, 2012, **12**, 4825–4841.

15 Q. Dai, T. Dai, L. Hou, L. Li, X. Bi, Y. Zhang and Y. Feng, Quantifying the impacts of emissions and meteorology on the interannual variations of air pollutants in major Chinese cities from 2015 to 2021, *Sci. China:Earth Sci.*, 2023, **66**(8), 1725–1737.

16 J. Hu and Y. Zhang, Reinforce the coordinated control of O_3 and $PM_{2.5}$ to continuously improve China's ambient air quality, *Chin. Sci. Bull.*, 2022, **67**, 1975–1977.

17 X. Feng, Y. Tian, Q. Xue, D. Song, F. Huang and Y. Feng, Measurement report: Spatiotemporal and policy-related variations of $PM_{2.5}$ composition and sources during 2015–2019 at multiple sites in a Chinese megacity, *Atmos. Chem. Phys.*, 2021, **21**, 16219–16235.

18 A. Liu, N. Sang, H. Duan, X. Yang, L. Wang, N. Nan, R. Chen and G. Qin, Atmospheric PM2.5-bound polycyclic aromatic hydrocarbons in China's four cities: Characterization, risk assessment, and epithelial-to-mesenchymal transition induced by PM2.5, *Atmos. Pollut. Res.*, 2021, **12**(7), 101122.

19 X. Wu, J. Xin, X. Zhang, R. Si, G. Liu, A. Li, T. Wen, Z. Liu, S. Wang, G. Fan, Y. Wang, L. Wang and W. Gao, Comparative research on visibility and light extinction of PM2.5 components during 2014–17 in the North China plain, *Atmos. Oceanic Sci. Lett.*, 2021, **14**, 100034.

20 G. Zhang, L. Jin, Z. Wang, J. Li, L. Ming, W. Yang, P. Fu, D. Liu and X. Li, PM2.5 in the Yangtze River Delta, China: Chemical compositions, seasonal variations, and regional pollution events, *Environ. Pollut.*, 2017, **223**, 200–212.

21 J. Sandradewi, A. S. H. Prévôt, E. Weingartner, R. Schmidhauser, M. Gysel and U. Baltensperger, A study of wood burning and traffic aerosols in an Alpine valley using a multi-wavelength Aethalometer, *Atmos. Environ.*, 2008, **42**, 101–112.

22 R. M. Healy, U. Sofowote, Y. Su, J. Debosz, M. Noble, C.-H. Jeong, J. M. Wang, N. Hilker, G. J. Evans, G. Doerksen, K. Jones and A. Munoz, Ambient measurements and source apportionment of fossil fuel and biomass burning black carbon in Ontario, *Atmos. Environ.*, 2017, **161**, 34–47.

23 A. Jing, B. Zhu, H. Wang, X. Yu, J. An and H. Kang, Source apportionment of black carbon in different seasons in the northern suburb of Nanjing, China, *Atmos. Environ.*, 2019, **201**, 190–200.

24 Y. Liu, C. Yan and M. Zheng, Source apportionment of black carbon during winter in Beijing, *Sci. Total Environ.*, 2018, **618**, 531–541.

25 S. Saarikoski, J. V. Niemi, M. Aurela, L. Pirjola, A. Kousa, T. Rönkkö and H. Timonen, Sources of black carbon at residential and traffic environments obtained by two source apportionment methods, *Atmos. Chem. Phys.*, 2021, **21**, 14851–14869.

26 T. Liao, K. Gui, W. Jiang, S. Wang, B. Wang, Z. Zeng, H. Che, Y. Wang and Y. Sun, Air stagnation and its impact on air quality during winter in Sichuan and Chongqing, southwestern China, *Sci. Total Environ.*, 2018, **635**, 576–585.

27 N. Zhang, Y. Qin and S. Xie, Spatial distribution of black carbon emissions in China, *Chin. Sci. Bull.*, 2013, **58**, 3830–3839.

28 H. Zhong, R.-J. Huang, C. Lin, W. Xu, J. Duan, Y. Gu, W. Huang, H. Ni, C. Zhu, Y. You, Y. Wu, R. Zhang, J. Ovadnevaite, D. Ceburnis and C. D. O'Dowd, Measurement report: On the contribution of long-distance transport to the secondary aerosol formation and aging, *Atmos. Chem. Phys.*, 2022, **22**, 9513–9524.

29 Y. Chen, J. Wenger, F. Yang, J. Cao, R. Huang, G. Shi, S. Zhang, M. Tian and H. Wang, Source characterization of urban particles from meat smoking activities in Chongqing, China using single particle aerosol mass spectrometry, *Environ. Pollut.*, 2017, **228**, 92–101.

30 J. Luo, J. Zhang, X. Huang, Q. Liu, B. Luo, W. Zhang, Z. Rao and Y. Yu, Characteristics, evolution, and regional differences of biomass burning particles in the Sichuan Basin, China, *J. Environ. Sci.*, 2020, **89**, 35–46.

31 Y. Wang, M. Hu, W. Hu, J. Zheng, H. Niu, X. Fang, N. Xu, Z. Wu, S. Guo, Y. Wu, W. Chen, S. Lu, M. Shao, S. Xie, B. Luo and Y. Zhang, Secondary Formation of Aerosols Under Typical High-Humidity Conditions in Wintertime Sichuan Basin, China: A Contrast to the North China Plain, *J. Geophys. Res.:Atmos.*, 2021, **126**(10), DOI: 10.1029/2021JD034560.

32 Y. Ma, S. Li, J. Zheng, A. Khalizov, X. Wang, Z. Wang and Y. Zhou, Size-resolved measurements of mixing state and cloud-nucleating ability of aerosols in Nanjing, China, *J. Geophys. Res.:Atmos.*, 2017, **122**, 9430–9450.

33 J. Y. Sun, C. Wu, D. Wu, C. Cheng, M. Li, L. Li, T. Deng, J. Z. Yu, Y. J. Li, Q. Zhou, Y. Liang, T. Sun, L. Song, P. Cheng, W. Yang, C. Pei, Y. Chen, Y. Cen, H. Nian and Z. Zhou, Amplification of black carbon light absorption induced by atmospheric aging: temporal variation at seasonal and diel scales in urban Guangzhou, *Atmos. Chem. Phys.*, 2020, **20**, 2445–2470.

34 W. Chen, X. Cao, H. Ran, T. Chen, B. Yang and X. Zheng, Concentration and source allocation of black carbon by AE-33 model in urban area of Shenzhen, southern China, *J. Environ. Health Sci. Eng.*, 2022, **20**, 469–483.

35 W. Lei, X. Li, Z. Yin, L. Zhang and W. Zhao, Pollution Characteristics and Source Apportionment of Black Carbon Aerosols during Spring in Beijing, *Toxics*, 2024, **12**, 202.

36 X. Liu, M. Zheng, Y. Liu, Y. Jin, J. Liu, B. Zhang, X. Yang, Y. Wu, T. Zhang, Y. Xiang, B. Liu and C. Yan, Intercomparison of equivalent black carbon (eBC) and elemental carbon (EC) concentrations with three-year continuous measurement in Beijing, China, *Environ. Res.*, 2022, **209**, 112791.

37 D. Paraskevopoulou, D. G. Kaskaoutis, G. Grivas, S. Bikkina, M. Tsagkaraki, I. M. Vrettou, K. Tavernaraki, K. Papoutsidaki, I. Stavroulas, E. Liakakou, A. Bougiatioti, K. Oikonomou, E. Gerasopoulos and N. Mihalopoulos, Brown carbon absorption and radiative effects under intense residential wood burning conditions in Southeastern Europe: New insights into the abundance and absorptivity of methanol-soluble organic aerosols, *Sci. Total Environ.*, 2023, **860**, 160434.

38 M. Savadkoohi, M. Pandolfi, O. V. Rattigan, X. Querol, A. Alastuey and P. K. Hopke, Multi-site comparison and source apportionment of equivalent Black Carbon mass concentrations (eBC) in the United States: Southern California Basin and Rochester, New York, *Atmos. Pollut. Res.*, 2025, **16**, 102340.

39 R. A. Sugrue, C. V. Preble, J. D. A. Butler, A. J. Redon-Gabel, P. Marconi, K. D. Shetty, L. A. L. Hill, A. M. Amezcua-Smith, B. R. Lukanov and T. W. Kirchstetter, The value of adding black carbon to community monitoring of particulate matter, *Atmos. Environ.*, 2024, **325**, 120434.

40 Y. Zhang, Y. Li, J. Guo, Y. Wang, D. Chen and H. Chen, The climatology and trend of black carbon in China from 12-year ground observations, *Clim. Dyn.*, 2019, **53**, 5881–5892.

41 Z. Shu, T. Zhao, Y. Liu, L. Zhang, M. Xiaodan, X. Kuang, Y. Li, Z. Huo, Q. Ding, X. Sun and L. Shen, Impact of deep basin terrain on PM2.5 distribution and its seasonality over the Sichuan Basin, Southwest China, *Environ. Pollut.*, 2022, **300**, 118944.

42 R. Hu, H. Wang, Y. Yin, B. Zhu, L. Xia, Z. Zhang and K. Chen, Measurement of ambient aerosols by single particle mass spectrometry in the Yangtze River Delta, China: Seasonal variations, mixing state and meteorological effects, *Atmos. Res.*, 2018, **213**, 562–575.

43 P. Kumar, K. Sharma, A. Malu, R. Rajak, A. Gupta, B. Baruah, S. Yadav, T. Angchuk, J. Sharma, R. K. Ranjan, A. K. Misra and N. Wanjari, Measurement report: Intra-annual variability of black carbon and brown carbon and their interrelation with meteorological conditions over Gangtok, Sikkim, *Atmos. Chem. Phys.*, 2024, **24**, 11585–11601.

44 A. Petzold, J. A. Ogren, M. Fiebig, P. Laj, S.-M. Li, U. Baltensperger, T. Holzer-Popp, S. Kinne, G. Pappalardo, N. Sugimoto, C. Wehrli, A. Wiedensohler and X.-Y. Zhang, Recommendations for reporting 'black carbon' measurements, *Atmos. Chem. Phys.*, 2013, **13**, 8365–8379.

45 M. Savadkoohi, M. Pandolfi, O. Favez, J.-P. Putaud, K. Eleftheriadis, M. Fiebig, P. K. Hopke, P. Laj, A. Wiedensohler, L. Alados-Arboledas, S. Bastian, B. Chazeau, Á. C. María, C. Colombi, F. Costabile, D. C. Green, C. Hueglin, E. Liakakou, K. Luoma, S. Listrani, N. Mihalopoulos, N. Marchand, G. Močnik, J. V. Niemi, J. Ondráček, J.-E. Petit, O. V. Rattigan, C. Reche, H. Timonen, G. Titos, A. H. Tremper, S. Vratolis, P. Vodička, E. Y. Funes, N. Zíková, R. M. Harrison, T. Petäjä, A. Alastuey and X. Querol, Recommendations for reporting equivalent black carbon (eBC) mass concentrations based on long-term pan-European in-situ observations, *Environ. Int.*, 2024, **185**, 108553.

46 L. Drinovec, G. Močnik, P. Zotter, A. S. H. Prévôt, C. Ruckstuhl, E. Coz, M. Rupakheti, J. Sciare, T. Müller, A. Wiedensohler and A. D. A. Hansen, The 'dual-spot' Aethalometer: an improved measurement of aerosol black carbon with real-time loading compensation, *Atmos. Meas. Tech.*, 2015, **8**, 1965–1979.

47 M. Savadkoohi, M. Pandolfi, C. Reche, J. V. Niemi, D. Mooibroek, G. Titos, D. C. Green, A. H. Tremper, C. Hueglin, E. Liakakou, N. Mihalopoulos, I. Stavroulas, B. Artiñano, E. Coz, L. Alados-Arboledas, D. Beddows, V. Riffault, J. F. De Brito, S. Bastian, A. Baudic, C. Colombi, F. Costabile, B. Chazeau, N. Marchand, J. L. Gómez-Amo, V. Estellés, V. Matos, E. Van Der Gaag, G. Gille, K. Luoma, H. E. Manninen, M. Norman, S. Silvergren, J.-E. Petit, J.-P. Putaud, O. V. Rattigan, H. Timonen, T. Tuch, M. Merkel, K. Weinhold, S. Vratolis, J. Vasilescu, O. Favez, R. M. Harrison, P. Laj, A. Wiedensohler, P. K. Hopke, T. Petäjä, A. Alastuey and X. Querol, The variability of mass concentrations and source apportionment analysis of equivalent black carbon across urban Europe, *Environ. Int.*, 2023, **178**, 108081.

48 Y. M. Qin, H. B. Tan, Y. J. Li, Z. J. Li, M. I. Schurman, L. Liu, C. Wu and C. K. Chan, Chemical characteristics of brown carbon in atmospheric particles at a suburban site near Guangzhou, China, *Atmos. Chem. Phys.*, 2018, **18**, 16409–16418.

49 L. Wu, C. Wu, T. Deng, D. Wu, M. Li, Y. J. Li and Z. Zhou, Field comparison of dual- and single-spot Aethalometers: equivalent black carbon, light absorption, Ångström exponent and secondary brown carbon estimations, *Atmos. Meas. Tech.*, 2024, **17**, 2917–2936.

50 R. Wang, S. Tao, Y. Balkanski, P. Ciais, O. Boucher, J. Liu, S. Piao, H. Shen, M. R. Vuolo, M. Valari, H. Chen, Y. Chen, A. Cozic, Y. Huang, B. Li, W. Li, G. Shen, B. Wang and Y. Zhang, Exposure to ambient black carbon derived from a unique inventory and high-resolution model, *Proc. Natl. Acad. Sci. U. S. A.*, 2014, **111**, 2459–2463.

51 J. Sandradewi, A. S. H. Prévôt, S. Szidat, N. Perron, M. R. Alfarra, V. A. Lanz, E. Weingartner and U. Baltensperger, Using Aerosol Light Absorption Measurements for the Quantitative Determination of Wood Burning and Traffic Emission Contributions to Particulate Matter, *Environ. Sci. Technol.*, 2008, **42**, 3316–3323.

52 A. Ångström, The parameters of atmospheric turbidity, *Tellus*, 1964, **16**, 64–75.

53 H. Moosmüller, R. K. Chakrabarty, K. M. Ehlers and W. P. Arnott, Absorption Ångström coefficient, brown carbon, and aerosols: basic concepts, bulk matter, and spherical particles, *Atmos. Chem. Phys.*, 2011, **11**, 1217–1225.

54 Y. Chen, S. Zhang, C. Peng, G. Shi, M. Tian, R.-J. Huang, D. Guo, H. Wang, X. Yao and F. Yang, Impact of the COVID-19 pandemic and control measures on air quality and aerosol light absorption in Southwestern China, *Sci. Total Environ.*, 2020, **749**, 141419.

55 E. M. E. Baramoussi, Y. Ren, C. Xue, I. Ouchen, V. Daële, P. Mercier, C. Chalumeau, F. L. E. Fur, P. Colin, A. Yahyaoui, O. Favez and A. Mellouki, Nearly five-year continuous atmospheric measurements of black carbon over a suburban area in central France, *Sci. Total Environ.*, 2023, **858**, 159905.

56 X. Fan, S. Ye, H. Zheng, B. Han, G. Zhang, Z. Zheng, X. Zhao, S. Kong, X. Wang and W. Yang, Source apportionment of black carbon using an advanced Aethalometer model in a typical industrial city of China, *J. Environ. Sci.*, 2025, **151**, 42–53.

57 M. R. Olson, M. Victoria Garcia, M. A. Robinson, P. Van Rooy, M. A. Dietenberger, M. Bergin and J. J. Schauer, Investigation of black and brown carbon multiple-wavelength-dependent light absorption from biomass and fossil fuel combustion source emissions, *J. Geophys. Res.:Atmos.*, 2015, **120**, 6682–6697.

58 Y. Zhang, Y. Han, L. Dong, X. Deng, D. Ye and S. Shao, Spatiotemporal variations and source on black carbon over Chongqing, China: Long-term changes and observational experiments, *Sci. Total Environ.*, 2024, **946**, 174127.

59 J. C. Corbin, H. Czech, D. Massabò, F. B. De Mongeot, G. Jakobi, F. Liu, P. Lobo, C. Mennucci, A. A. Mensah, J. Orasche, S. M. Pieber, A. S. H. Prévôt, B. Stengel, L.-L. Tay, M. Zanatta, R. Zimmermann, I. El Haddad and M. Gysel, Infrared-absorbing carbonaceous tar can dominate light absorption by marine-engine exhaust, *npj Clim. Atmos. Sci.*, 2019, **2**, 12.

60 A. Helin, A. Virkkula, J. Backman, L. Pirjola, O. Sippula, P. Aakko-Saksa, S. Väätäinen, F. Mylläri, A. Järvinen, M. Bloss, M. Aurela, G. Jakobi, P. Karjalainen, R. Zimmermann, J. Jokiniemi, S. Saarikoski, J. Tissari, T. Rönkkö, J. V. Niemi and H. Timonen, Variation of Absorption Ångström Exponent in Aerosols From Different Emission Sources, *J. Geophys. Res.:Atmos.*, 2021, **126**, e2020JD034094.

61 K. E. Yttri, A. Bäcklund, F. Conen, S. Eckhardt, N. Evangeliou, M. Fiebig, A. Kasper-Giebl, A. Gold, H. Gundersen, C. L. Myhre, S. M. Platt, D. Simpson, J. D. Surratt, S. Szidat, M. Rauber, K. Tørseth, M. A. Ytre-Eide, Z. Zhang and W. Aas, Composition and sources of carbonaceous aerosol in the European Arctic at Zeppelin Observatory, Svalbard (2017 to 2020), *Atmos. Chem. Phys.*, 2024, **24**, 2731–2758.

62 Y. Wang, B. de Foy, J. J. Schauer, M. R. Olson, Y. Zhang, Z. Li and Y. Zhang, Impacts of regional transport on black carbon in Huairou, Beijing, China, *Environ. Pollut.*, 2017, **221**, 75–84.

63 P. Zotter, H. Herich, M. Gysel, I. El-Haddad, Y. Zhang, G. Močnik, C. Hüglin, U. Baltensperger, S. Szidat and A. S. H. Prévôt, Evaluation of the absorption Ångström exponents for traffic and wood burning in the Aethalometer-based source apportionment using radiocarbon measurements of ambient aerosol, *Atmos. Chem. Phys.*, 2017, **17**, 4229–4249.

64 Y. Chen, G. Zhi, Y. Feng, D. Liu, G. Zhang, J. Li, G. Sheng and J. Fu, Measurements of Black and Organic Carbon Emission Factors for Household Coal Combustion in China: Implication for Emission Reduction, *Environ. Sci. Technol.*, 2009, **43**, 9495–9500.

65 W. Wang, N. Khanna, J. Lin and X. Liu, Black carbon emissions and reduction potential in China: 2015–2050, *J. Environ. Manage.*, 2023, **329**, 117087.

66 W. Zhao, Y. Zhao, Y. Zheng, D. Chen, J. Xin, K. Li, H. Che, Z. Li, M. Ma and Y. Hang, Long-term variability in black carbon emissions constrained by gap-filled absorption aerosol optical depth and associated premature mortality in China, *Atmos. Chem. Phys.*, 2024, **24**, 6593–6612.

67 W. Zhang, Z. Lu, Y. Xu, C. Wang, Y. Gu, H. Xu and D. G. Streets, Black carbon emissions from biomass and coal in rural China, *Atmos. Environ.*, 2018, **176**, 158–170.

68 A. Mousavi, M. H. Sowlat, S. Hasheminassab, A. Polidori and C. Sioutas, Spatio-temporal trends and source apportionment of fossil fuel and biomass burning black carbon (BC) in the Los Angeles Basin, *Sci. Total Environ.*, 2018, **640–641**, 1231–1240.

69 M. Becerril-Valle, E. Coz, A. S. H. Prévôt, G. Močnik, S. N. Pandis, A. M. Sánchez De La Campa, A. Alastuey,

E. Díaz, R. M. Pérez and B. Artíñano, Characterization of atmospheric black carbon and co-pollutants in urban and rural areas of Spain, *Atmos. Environ.*, 2017, **169**, 36–53.

70 A. Mousavi, M. H. Sowlat, C. Lovett, M. Rauber, S. Szidat, R. Boffi, A. Borgini, C. De Marco, A. A. Ruprecht and C. Sioutas, Source apportionment of black carbon (BC) from fossil fuel and biomass burning in metropolitan Milan, Italy, *Atmos. Environ.*, 2019, **203**, 252–261.

71 X. Peng, M. Liu, Y. Zhang, Z. Meng, V. Achal, T. Zhou, L. Long and Q. She, The characteristics and local-regional contributions of atmospheric black carbon over urban and suburban locations in Shanghai, China, *Environ. Pollut.*, 2019, **255**, 113188.

72 J. Sun, Z. Wang, W. Zhou, C. Xie, C. Wu, C. Chen, T. Han, Q. Wang, Z. Li, J. Li, P. Fu, Z. Wang and Y. Sun, Measurement report: Long-term changes in black carbon and aerosol optical properties from 2012 to 2020 in Beijing, China, *Atmos. Chem. Phys.*, 2022, **22**, 561–575.

73 J. Zhang, Y. Yao, C. Xiao, Y. Gu, X. Jin, P. Wang and L. Zhao, The pollution characterization of black carbon aerosols in the southwest suburb of beijing from 2013 to 2019, *Atmos. Pollut. Res.*, 2023, **14**, 101669.

74 J. Rovira, M. Savadkoohi, G. I. Chen, G. Močnik, W. Aas, L. Alados-Arboledas, B. Artiñano, M. Aurela, J. Backman, S. Banerji, D. Beddows, B. Brem, B. Chazeau, M. C. Coen, C. Colombi, S. Conil, F. Costabile, E. Coz, J. F. De Brito, K. Eleftheriadis, O. Favez, H. Flentje, E. Freney, A. Gregorič, M. Gysel-Beer, R. Harrison, C. Hueglin, A. Hyvärinen, M. Ivančič, A.-C. Kalogridis, H. Keernik, G. Konstantinos, P. Laj, E. Liakakou, C. Lin, S. Listrani, K. Luoma, M. Maasikmets, H. E. Manninen, N. Marchand, S. M. Dos Santos, S. Mbengue, N. Mihalopoulos, D. Nicolae, J. V. Niemi, M. Norman, J. Ovadnevaite, J.-E. Petit, S. Platt, A. S. H. Prévôt, M. Pujadas, J.-P. Putaud, V. Riffault, M. Rigler, M. Rinaldi, J. Schwarz, S. Silvergren, E. Teinemaa, K. Teinilä, H. Timonen, G. Titos, A. Tobler, J. Vasilescu, S. Vratolis, K. E. Yttri, E. Yubero, N. Zíková, A. Alastuey, T. Petäjä, X. Querol, J. Yus-Díez and M. Pandolfi, A European aerosol phenomenology – 9: Light absorption properties of carbonaceous aerosol particles across surface Europe, *Environ. Int.*, 2025, **195**, 109185.

75 K. P. Wyche, R. L. Cordell, L. Smith M, K. L. Smallbone, P. Lyons, S. M. L. Hama, P. S. Monks, J. Staelens, J. Hofman, C. Stroobants, E. Roekens, G. P. A. Kos, E. P. Weijers, P. Panteliadis and M. B. A. Dijkema, The spatio-temporal evolution of black carbon in the North-West European 'air pollution hotspot', *Atmos. Environ.*, 2020, **243**, 117874.

76 O. V. Rattigan, K. Civerolo, P. Doraiswamy, H. D. Felton and P. K. Hopke, Long Term Black Carbon Measurements at Two Urban Locations in New York, *Aerosol Air Qual. Res.*, 2013, **13**, 1181–1196.

77 H. Hayami, S. Saito and S. Hasegawa, Spatiotemporal Variations of Fine Particulate Organic and Elemental Carbons in Greater Tokyo, *Asian J. Atmos. Environ.*, 2019, **13**, 161–170.

78 U. C. Dumka, D. G. Kaskaoutis, S. Tiwari, P. D. Safai, S. D. Attri, V. K. Soni, N. Singh and N. Mihalopoulos, Assessment of biomass burning and fossil fuel contribution to black carbon concentrations in Delhi during winter, *Atmos. Environ.*, 2018, **194**, 93–109.

79 U. C. Dumka, D. G. Kaskaoutis, P. C. S. Devara, R. Kumar, S. Kumar, S. Tiwari, E. Gerasopoulos and N. Mihalopoulos, Year-long variability of the fossil fuel and wood burning black carbon components at a rural site in southern Delhi outskirts, *Atmos. Res.*, 2019, **216**, 11–25.

80 J. Su, R. Zhang, B. Liu, M. Tong, S. Xiao, X. Wang, Q. Zhao, W. Song, D. Talifu and X. Wang, Seasonal and Day–Night Variations in Carbonaceous Aerosols and Their Light-Absorbing Properties in Guangzhou, China, *Atmosphere*, 2023, **14**, 1545.

81 D. Cheng, C. Wu, L. Song, T. L. Sun and A. M. Liu, Comparative study on the characteristics of black carbon aerosol in urban and suburban areas of Shenzhen, *China Environ. Sci.*, 2018, **38**, 1653–1662.

82 C. Peng, F. Yang, M. Tian, G. Shi, L. Li, R.-J. Huang, X. Yao, B. Luo, C. Zhai and Y. Chen, Brown carbon aerosol in two megacities in the Sichuan Basin of southwestern China: Light absorption properties and implications, *Sci. Total Environ.*, 2020, **719**, 137483.

83 C. He, X. Niu, Z. Ye, Q. Wu, L. Liu, Y. Zhao, J. Ni, B. Li and J. Jin, Black carbon pollution in China from 2001 to 2019: Patterns, trends, and drivers, *Environ. Pollut.*, 2023, **324**, 121381.

84 K. Wu, Y. Wang, Y. Qiao, Y. Liu, S. Wang, X. Yang, H. Wang, Y. Lu, X. Zhang and Y. Lei, Drivers of 2013–2020 ozone trends in the Sichuan Basin, China: Impacts of meteorology and precursor emission changes, *Environ. Pollut.*, 2022, **300**, 118914.

85 X. Yang, K. Wu, Y. Lu, S. Wang, Y. Qiao, X. Zhang, Y. Wang, H. Wang, Z. Liu, Y. Liu and Y. Lei, Origin of regional springtime ozone episodes in the Sichuan Basin, China: Role of synoptic forcing and regional transport, *Environ. Pollut.*, 2021, **278**, 116845.

86 L. Chen, J. Zhang, X. Huang, H. Li, G. Dong and S. Wei, Characteristics and pollution formation mechanism of atmospheric fine particles in the megacity of Chengdu, China, *Atmos. Res.*, 2022, **273**, 106172.

87 L. Kong, J. Xin, Z. Liu, K. Zhang, G. Tang, W. Zhang and Y. Wang, The PM2.5 threshold for aerosol extinction in the Beijing megacity, *Atmos. Environ.*, 2017, **167**, 458–465.

88 G. Zhang, L. Peng, X. Lian, Q. Lin, X. Bi, D. Chen, M. Li, L. Li, X. Wang and G. Sheng, An Improved Absorption Ångström Exponent (AAE)-Based Method for Evaluating the Contribution of Light Absorption from Brown Carbon with a High-Time Resolution, *Aerosol Air Qual. Res.*, 2019, **19**, 15–24.

89 L. Zhang, Z. Luo, W. Du, G. Li, G. Shen, H. Cheng and S. Tao, Light absorption properties and absorption emission factors for indoor biomass burning, *Environ. Pollut.*, 2020, **267**, 115652.

90 D. Liu, C. He, J. P. Schwarz and X. Wang, Lifecycle of light-absorbing carbonaceous aerosols in the atmosphere, *npj Clim. Atmos. Sci.*, 2020, **3**, 40.
91 A. Laskin, J. Laskin and S. A. Nizkorodov, Chemistry of Atmospheric Brown Carbon, *Chem. Rev.*, 2015, **115**, 4335–4382.
92 G. Park, K. Kim, T. Park, S. Kang, J. Ban, S. Choi, D.-G. Yu, S. Lee, Y. Lim, S. Kim, J. Lee, J.-H. Woo and T. Lee, Characterizing Black Carbon Emissions from Gasoline, LPG, and Diesel Vehicles via Transient Chassis-Dynamometer Tests, *Appl. Sci.*, 2020, **10**, 5856.
93 Z. Bao, Y. Liu, L. Meng, Y. Han, M. Tian, G. Shi, Q. Wang, Y. Huang, C. Peng, B. Luo, W. Zhang, H. Wang, J. Cao, F. Yang and Y. Chen, Evaluating the Effects of Biomass Burning on Severe Haze Formation in a Megacity of Sichuan Basin, Southwestern China, *J. Geophys. Res.:Atmos.*, 2025, **130**, e2024JD042516.
94 J. Ding, W. Huang, J. Zhao, L. Li, G. Xiong, C. Jiang, D. Ye, D. Li, J. Wang, J. Yu and R. Liu, Characteristics and source origins of carbonaceous aerosol in fine particulate matter in a megacity, Sichuan Basin, southwestern China, *Atmos. Pollut. Res.*, 2022, **13**, 101266.
95 A. Minderytė, J. Pauraite, V. Dudoitis, K. Plauškaitė, A. Kilikevičius, J. Matijošius, A. Rimkus, K. Kilikevičienė, D. Vainorius and S. Byčenkienė, Carbonaceous aerosol source apportionment and assessment of transport-related pollution, *Atmos. Environ.*, 2022, **279**, 119043.
96 Y. Zhang, Z. Shi, Y. Wang, L. Liu, J. Zhang, J. Li, Y. Xia, X. Ding, D. Liu, S. Kong, H. Niu, P. Fu, X. Zhang and W. Li, Fine particles from village air in northern China in winter: Large contribution of primary organic aerosols from residential solid fuel burning, *Environ. Pollut.*, 2021, **272**, 116420.
97 Q. Luo, X. Liu, K. Wang and C. Liu, Increasingly frequent co-occurrence of drought or pluvial in multiple tributaries of the Yangtze River basin, *J. Hydrol.*, 2024, **633**, 131035.
98 X. Wang, S. Guo, S. Zhong, M. Wang and X. Xiang, Flood Season Division Using Statistical Analysis Methods and Verifying by Regional Rainy Characteristics, *Water*, 2024, **16**, 3677.
99 B. Romshoo, T. Müller, S. Pfeifer, J. Saturno, A. Nowak, K. Ciupek, P. Quincey and A. Wiedensohler, Optical properties of coated black carbon aggregates: numerical simulations, radiative forcing estimates, and size-resolved parameterization scheme, *Atmos. Chem. Phys.*, 2021, **21**, 12989–13010.
100 C. Wu, D. Wu and J. Z. Yu, Quantifying black carbon light absorption enhancement with a novel statistical approach, *Atmos. Chem. Phys.*, 2018, **18**, 289–309.
101 S. Polinov, R. Bookman and N. Levin, A Global Assessment of Night Lights as an Indicator for Shipping Activity in Anchorage Areas, *Remote Sens.*, 2022, **14**, 1079.
102 H. Murata, R. Shibasaki, N. Imura and K. Nishinari, Identifying the operational status of container terminals from high-resolution nighttime-light satellite image for global supply chain network optimization, *Front. Remote Sens.*, 2023, **4**, 1229745.
103 E. Murphy and E. A. King, An assessment of residential exposure to environmental noise at a shipping port, *Environ. Int.*, 2014, **63**, 207–215.
104 D. Ji, W. Gao, W. Maenhaut, J. He, Z. Wang, J. Li, W. Du, L. Wang, Y. Sun, J. Xin, B. Hu and Y. Wang, Impact of air pollution control measures and regional transport on carbonaceous aerosols in fine particulate matter in urban Beijing, China: insights gained from long-term measurement, *Atmos. Chem. Phys.*, 2019, **19**, 8569–8590.
105 R. D. Kutzner, E. Von Schneidemesser, F. Kuik, J. Quedenau, E. C. Weatherhead and J. Schmale, Long-term monitoring of black carbon across Germany, *Atmos. Environ.*, 2018, **185**, 41–52.
106 O. V. Rattigan, A. C. Carpenter, H. D. Felton and K. L. Civerolo, Optical carbon analysis on Teflon filters from the FRM network in New York, *Atmos. Pollut. Res.*, 2021, **12**, 101163.
107 Y. Cheng, S. C. Lee, Y. Gao, L. Cui, W. Deng, J. Cao, Z. Shen and J. Sun, Real-time measurements of PM2.5, PM10–2.5, and BC in an urban street canyon, *Particuology*, 2015, **20**, 134–140.
108 D. Carslaw, S. Beevers, K. Ropkins and M. Bell, Detecting and quantifying aircraft and other on-airport contributions to ambient nitrogen oxides in the vicinity of a large international airport, *Atmos. Environ.*, 2006, **40**, 5424–5434.
109 D. C. Carslaw, S. D. Beevers and J. E. Tate, Modelling and assessing trends in traffic-related emissions using a generalised additive modelling approach, *Atmos. Environ.*, 2007, **41**, 5289–5299.
110 S. K. Grange, A. C. Lewis and D. C. Carslaw, Source apportionment advances using polar plots of bivariate correlation and regression statistics, *Atmos. Environ.*, 2016, **145**, 128–134.
111 R. P. Pokhrel, N. L. Wagner, J. M. Langridge, D. A. Lack, T. Jayarathne, E. A. Stone, C. E. Stockwell, R. J. Yokelson and S. M. Murphy, Parameterization of single-scattering albedo (SSA) and absorption Ångström exponent (AAE) with EC/OC for aerosol emissions from biomass burning, *Atmos. Chem. Phys.*, 2016, **16**, 9549–9561.
112 S. Török, V. B. Malmborg, J. Simonsson, A. Eriksson, J. Martinsson, M. Mannazhi, J. Pagels and P.-E. Bengtsson, Investigation of the absorption Ångström exponent and its relation to physicochemical properties for mini-CAST soot, *Aerosol Sci. Technol.*, 2018, **52**, 757–767.
113 M. Li, H. Liu, G. Geng, C. Hong, F. Liu, Y. Song, D. Tong, B. Zheng, H. Cui, H. Man, Q. Zhang and K. He, Anthropogenic emission inventories in China: a review, *Natl. Sci. Rev.*, 2017, **4**, 834–866.
114 B. Ambade, T. K. Sankar, A. S. Panicker, A. S. Gautam and S. Gautam, Characterization, seasonal variation, source apportionment and health risk assessment of black carbon over an urban region of East India, *Urban Clim.*, 2021, **38**, 100896.
115 C. Xie, Y. He, L. Lei, W. Zhou, J. Liu, Q. Wang, W. Xu, Y. Qiu, J. Zhao, J. Sun, L. Li, M. Li, Z. Zhou, P. Fu, Z. Wang and Y. Sun, Contrasting mixing state of black carbon-

containing particles in summer and winter in Beijing, *Environ. Pollut.*, 2020, **263**, 114455.

116 Y. Zhang, J. Wang, N. Wu, X. Ouyang, G. Li, Y. Cheng, Q. Zhang, A. Ding and H. Su, The Contribution of Black Carbon-Containing Particles to $PM_{2.5}$: Variability, Drivers, and Impacts, *Environ. Sci. Technol.*, 2025, **59**, 5155–5163.

117 S. Chen, H. Wang, K. Lu, L. Zeng, M. Hu and Y. Zhang, The trend of surface ozone in Beijing from 2013 to 2019: Indications of the persisting strong atmospheric oxidation capacity, *Atmos. Environ.*, 2020, **242**, 117801.

118 Z. Tan, K. Lu, M. Jiang, R. Su, H. Wang, S. Lou, Q. Fu, C. Zhai, Q. Tan, D. Yue, D. Chen, Z. Wang, S. Xie, L. Zeng and Y. Zhang, Daytime atmospheric oxidation capacity in four Chinese megacities during the photochemically polluted season: a case study based on box model simulation, *Atmos. Chem. Phys.*, 2019, **19**, 3493–3513.

119 R. C. Cohen and J. G. Murphy, Photochemistry of NO2 in Earth's Stratosphere: Constraints from Observations, *Chem. Rev.*, 2003, **103**, 4985–4998.